THE ASTROPHYSICAL JOURNAL, 361:1–20, 1990 September 20

THE SURFACE BRIGHTNESS TEST FOR THE EXPANSION OF THE UNIVERSE. II. RADII, SURFACE BRIGHTNESS, AND ABSOLUTE MAGNITUDE CORRELATIONS FOR NEARBY E GALAXIES

ALLAN SANDAGE[1]
The Observatories of the Carnegie Institution of Washington
AND
JEAN-MARC PERELMUTER
The Johns Hopkins University, and Space Telescope Science Institute
Received 1989 September 13; accepted 1990 March 20

ABSTRACT

The correlation between absolute magnitude and surface brightness, averaged over a series of areas defined by metric (rather than isophotal) radii, is studied using E galaxies in the Virgo, Fornax, and Coma clusters, and in four additional samples of bright nearby field galaxies. The work is a calibration step in preparation for the Tolman $(1 + z)^4$ surface brightness test for the reality of the expansion. As known before, and as is seen in the present data, the average surface brightness is strongly correlated with absolute brightness for giant galaxies. Galaxies brighter than $M_B \sim -20$ have fainter average surface brightness values as the total galaxy luminosity increases.

The lack of a constant average surface brightness with changing absolute magnitude for bright E galaxies shows that Hubble's $m \sim -5 \log r''$ scaling law is not correct over the first few brightest magnitudes of the E luminosity function. Therefore measurements will be required of the $\langle SB \rangle$ over a *range* of M_T in distant clusters so as to reduce the $\langle SB \rangle$ data to "standard conditions" before searching for the Tolman $(1 + z)^4$ cosmological test signal. The purpose of the present paper is to calibrate the correlation between M_T and $\langle SB \rangle$ using local samples. In the samples studied here the dispersion in the $\langle SB \rangle$ distributions, after reducing the data to absolute magnitude $M_B = -22$ is ~ 0.5 mag. This value is smaller than the 1.8 mag Tolman $(1 + z)^4$ factor, even at the modest redshift of $z = 0.5$, showing that the Tolman test is feasible in practice as well as in principle.

Subject headings: cosmology — galaxies: clustering — galaxies: photometry

I. INTRODUCTION

It was shown in Paper I of this series (Sandage and Perelmuter 1990, hereafter SP90) that the measurements of sizes and flux levels of galaxies at large redshifts required for the Tolman (1930, 1934) surface brightness (hereinafter SB) test for the reality of the expansion are feasible with the present technology using existing ground-based telescopes. However, the requirement that the test be practical depends on whether the dispersion in surface brightness of the galaxies at a particular absolute magnitude in a particular galaxy sample is small compared with the predicted $(1 + z)^4$ shift in $\langle SB \rangle$.

The purpose of the present paper is to determine the dispersion in $\langle SB \rangle$ after the data have been reduced to a common absolute magnitude, thereby taking out the systematic variation of $\langle SB \rangle$ with $M_{B(T)}$. To determine this systematic variation we analyze data for elliptical galaxies in the Virgo, Fornax, and Coma clusters and in the general field. The field samples are taken from the second edition of the Revised Shapley-Ames Catalog (Sandage and Tammann 1987, hereafter RSA2), from the list by Sadler (1984), and from the galaxies studied by Thomsen and Frandsen (1983) and by Djorgovski and Davis (1987). The data are discussed using measures of both the effective radius and the Petrosian $r(\eta)$ radii determined by the methods developed in Paper I. The data in this and in Paper III to eventually follow have been taken from Oemler (1974, 1976), Fraser (1977), King (1978), Schombert (1986), Ichikawa, Wakamtsu, and Okamura (1986), Jedrzejewski (1987), Caldwell (1987), Vigroux *et al.* (1988), and Ferguson (1989).

II. PROCEDURE

For each galaxy in our sample a measured intensity profile $I(r_i)$ exists in the literature, expressed as a series of surface brightness values at various radii r_i. The data are most often listed along the major axis, but sometimes along the "effective" axis $(ab)^{1/2}$. The measurements begin at some finite radius, typically $\sim 3''$ from the center. As described in Paper I, a fitting function from the Oemler (1976) family has been used to extend the measured $I(r_i)$ values to the center (where no data exist), permitting a complete calculation of the growth curve and the Petrosian $\eta(r)$ function to be made by numerical integration.

Various types of measurements have been made from these integrations, as shown in the example in Figure 1 where the SB profile in B for NGC 4473 is shown as open circles from data by Vigroux *et al.* (1988). This profile is extrapolated inward by fitting an Oemler function to the listed data points that are closest to the center. The magnitude scale in B for the calculated $m(r)$ growth curve is along the outer right-hand ordinate; that for the $\eta(r)$ function is along the inner right hand ordinate.

The $m(r)$ growth curves calculated in this way could be checked for many galaxies using literature values of aperture

[1] Associated with the Department of Physics and Astronomy of The John Hopkins University, and the Space Telescope Science Institute, Baltimore, Maryland, when most of the work for this paper was done.

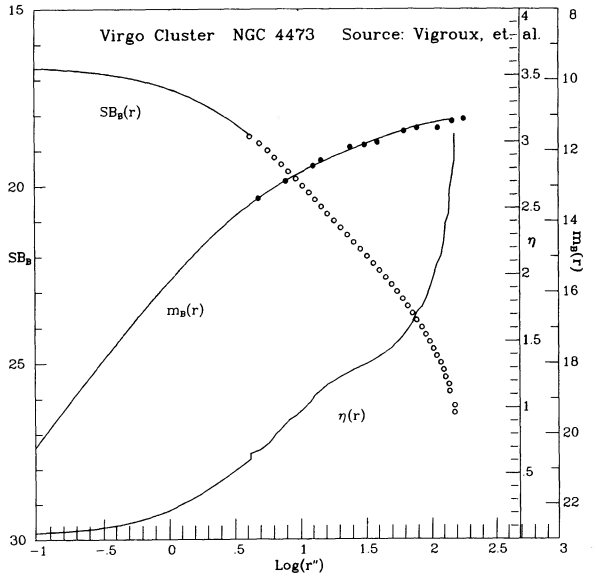

FIG. 1.—Type of data obtained for each galaxy in our sample, using as an example the profile photometry for NGC 4473 from Vigroux *et al.* (1988). Curves show, respectively, the luminosity profile (in B magnitudes arcsec^{-2}) using the scale along the left ordinate, the $m_B(r)$ growth curve calculated from the profile, and the Petrosian $\eta(r)$ function calculated as described in Paper I (SP90). Directly observed values of the integrated magnitude through various apertures, taken from the literature, are shown along the growth curve.

photometry at a number of measured radii, as listed, for example, by Longo and de Vaucouleurs (1983, 1985). A sample of the aperture photometry for NGC 4473 at several measured aperture sizes are shown in Figure 1 as filled circles, plotted along the calculated $m(r)$ curve. This diagram shows the excellent agreement between the directly measured aperture photometry for NGC 4473 and the $m(r)$ curve that we have calculated from the $I(r)$ profile data.

Such agreement was not always obtained for some of the galaxies in our data set. Often there is a small systematic offset in the zero point of the magnitudes. Without doubt, the principal reason for the offset is the error made by integrating the $I(r)$ distribution using circular apertures, thereby neglecting the flattening for noncircular E galaxies. One should use appropriate elliptical apertures and the appropriate complete $I(r, \theta)$ distributions at all azimuth angles, such as done by Djorgovski and Davis (1987). But the correction is small. From the discussion in the RC2 (de Vaucouleurs, de Vaucouleurs, and Corwin 1977, § 3.3*f*) the correction to a $\langle SB \rangle$ calculated with circular rather than elliptical apertures is shown to be 2.75 $(\log a/b)^2$, in magnitudes. For an E5 galaxy where $a/b = 2$ (such large flattenings are rare in our sample) the correction amounts to only ~ 0.3 mag, which, as we shall see in Figure 16 later, is negligible compared with the observed scatter in the data. We have neglected this ellipticity effect, but we *have* applied the observed zero-point offsets to the calculated $m(r)$ curves when appropriate and when the necessary photoelectric aperture data are available.

Note that the Petrosian $\eta(r)$ curves are unaffected by constant zero-point offsets in $m(r)$ at all r because $\eta(r)$ is a ratio. Therefore, the effective radii (r_e) as well as the η radii, $r(\eta)$, are also unaffected by simply a change in the $m(r)$ zero point.

We have calculated the B_T total magnitude for each galaxy in the sample by extrapolating the corrected $m(r)$ growth curve to $r = \infty$ by fitting one of the $m(r)$ template growth curves from Paper I to the calculated $m(r)$ shape over the radii range covered by the data. Figure 1 for NGC 4473 shows $B_T = 11.00$ mag from this extrapolation. The effective radius read from the $m(r)$ curve in Figure 1 at $B = 11.75$ is $r_e = 35''$, giving the surface brightness, *averaged over this effective radius*, to be $\langle SB \rangle_e = 20.74$ B magnitudes per square arc second.

Various Petrosian radii can be read directly from the $\eta(r)$ curve in an obvious way. The radii at which η has values of 1.3, 1.5, 1.7, 2.0, 2.5, and 3.0 mag arcsec^{-2} for NGC 4473 in Figure 1 are 26", 44", 78", 102", 132", and 155", and as such are listed in Table 1 discussed later. The SB averaged over these $r(\eta)$ radii can then be calculated at various $r(\eta)$ radii for each of the galaxies we have used.

Systematic errors in the $\eta(r)$ curves, and hence in $r(\eta)$ and $\langle SB \rangle_\eta$, exist due to the error which is made in the extrapolation of the SB profile into the center. Figure 2 shows the result of varying the extrapolated value of $B(0)$ by about 2 mag for four galaxies in the sample discussed in the following paper. The resulting variations in the $\eta(r)$ curve are shown in the right-hand panels. For small η values the variation in the shape of the $\eta(r)$ curve is, of course, larger than for $\eta > 1.5$ mag arcsec^{-2}, because the error due to errors in $B(0)$ becomes diluted as the $\eta(r)$ integration proceeds outward due to the increasing numerical value of the integral. A typical error in $r(\eta)$ at $\eta = 1.3$ mag arcsec^{-2} is $\Delta \log r(1.3) \sim 0.2$ when there is a difference of 2 mag in the estimate of $B(0)$ at the center. By the time η reaches ~ 2 mag arcsec^{-2}, the value of the integral giving $\langle SB(r) \rangle$ is so large that the error in $\log r(\eta)$ is less than $\Delta \log r(\eta) = 0.1$ even for the largest reasonable error we have made in $B(0)$ for most galaxies in our sample.

III. DATA FOR E AND S0 GALAXIES FROM FIVE SEPARATE SAMPLES

Data on the intensity profiles, $I(r)$, needed to calculate $\eta(r)$ values [and thereby $r(\eta)$ and $\langle SB \rangle_\eta$] have been obtained from the literature sources mentioned earlier for the three data samples comprising the Virgo, Fornax, and Coma clusters. Additional data on r_e and $m_{B(e)}$ for the Sadler (1984) field galaxy sample are contained in her tables. Data on r_e and B_e for the E galaxies in the RSA2 (Sandage and Tammann 1987), constituting our fifth sample, have been adopted from the listing in the RC2 (de Vaucouleurs, de Vaucouleurs, and Corwin 1977).

Data for the three cluster samples are given in Tables 1–3. Listed in the heading for each galaxy are the total absolute magnitude $M_{B(T)}$, the effective angular radii, r_e, in arc seconds, the effective apparent magnitude $B_e = B_T + 0.75$, and the average effective surface brightness (averaged over a circle of radius r_e). In the body of the tables are also listed the $r(\eta)$ radii (in arc seconds) obtained from the $\eta(r)$ curves read at our adopted discrete reading points, the B magnitude inside radius $r(\eta)$, and the resulting calculated average surface brightness $\langle SB \rangle_\eta$ within these radii. Apparent magnitudes have been changed to absolute magnitudes by adopting distance moduli of $m - M = 31.7$ for the Virgo cluster (Sandage and Tammann 1982*a*, *b*, 1985; Tammann and Sandage 1985, 1990), $m - M = 31.9$ for Fornax (Sandage and Tammann 1985; Ferguson and Sandage 1988), and $m - M = 35.5$ for Coma (Tammann and Sandage 1985, Table 5; Tammann 1986). Fornax cluster data, where only the effective parameters are available from either Caldwell (1987) or from the extensive catalog by Ferguson (1989), are set out in Table 2A. The first 31 entries of this table are due to Caldwell. The remaining

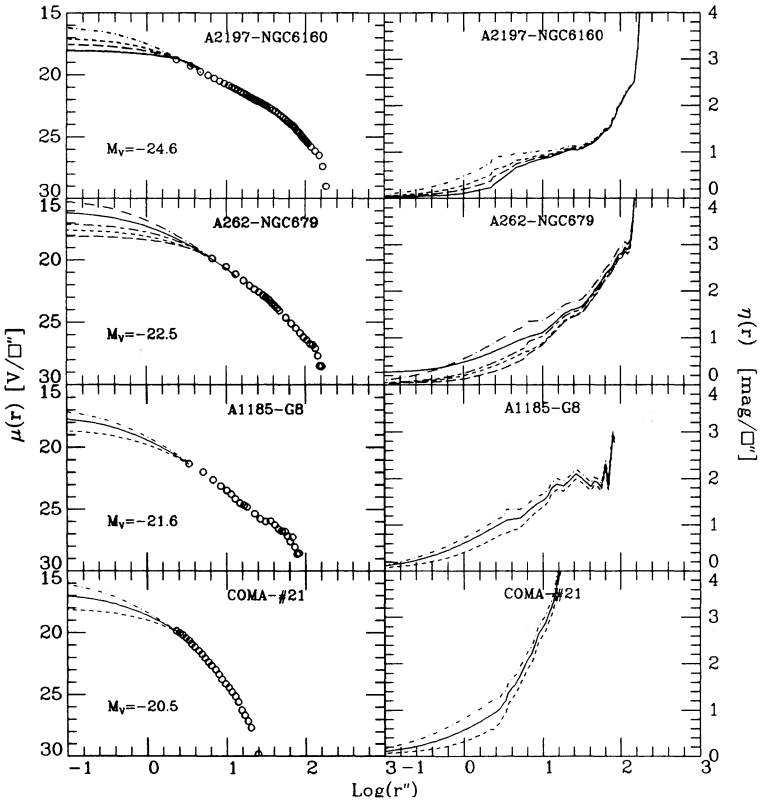

FIG. 2.—Illustration of the errors which are generated in the Pertrosian $\eta(r)$ radii caused by an error in extrapolating the profile data to the center to obtain $B(0)$ with which to begin the integration for $\eta(r)$. Left-hand panels show the observed intensity profiles (in magnitudes) as open circles, to which various extrapolations to the center are fitted; right-hand panels show the resulting families of $\eta(r)$ curves.

entries are due to Ferguson using his FCC (Fornax Cluster Catalog) numbers.

The data for the Coma cluster in Table 3 are based on measurements by Oemler (1976) for which he generously supplied his detailed data for the $I(r)$ profiles in digital form with which we performed the necessary integrations to obtain the equivalent of Figure 1 for each of his galaxies. Data on the absolute magnitudes and the effective photometric parameters for the galaxies measured by Sadler (1984) are set out in Table 4. Her listed B_T total magnitudes have been changed to absolute magnitudes in column (3) using the adopted distance modulus values in column (2), calculated from the redshift corrected to the centroid of the Local Group, and then using a Hubble constant of $H_0 = 50$ km s^{-1} Mpc^{-1}. Columns (4)–(6) give the effective B_e apparent magnitudes, the effective radii in arc seconds, and the resulting effective average surface brightness $\langle SB \rangle_e$.

Similar data for the E galaxies listed in the binning table in Part III of the RSA2 are listed in Table 5 using the $\langle SB \rangle_e$ values set out in the RC2. Many of the Table 5 (mostly field) galaxies were also used by Binggeli, Sandage, and Tarenghi (1984, hereafter BST) to define the bright sample in their Figure 8 for the $\langle SB \rangle$–absolute magnitude correlation. However, the photometric data used there were derived by BST from an independent evaluation of available literature data on aperture photometry rather than taking the $\langle SB \rangle_e$ values from the RC2. The reductions by BST were, then, independent of the listings in the RC2 which we use here in Table 5. Hence, the data in Tables 1–5 are largely independent of those used by BST for their Figure 8. The decision to use different data sets here to study the $\langle SB \rangle$, M correlation (Figs. 11 and 12 in later sections) was made to better determine the reliability of the $\langle SB \rangle$–absolute magnitude correlation.

IV. VARIATION OF THE EFFECTIVE RADIUS AND THE PETROSIAN RADII WITH ABSOLUTE MAGNITUDE FOR E GALAXIES

a) Hubble's Scaling Law

The data from Table 1 are plotted in Figure 3 to show the variation of the linear radii, R_e, with $M_{B(T)}$ for Virgo cluster. The metric radii are in parsecs using $D = 21.9$ Mpc ($m - M = 31.7$) for Virgo. The line of slope 5, zero-pointed at SB = 19 mag sec^{-2}, is shown. The two branches of the R_e, $M_{B(T)}$ relation, meeting near $M_{B(T)} = -20$, each with a slope that differs from 5, are evident.

The combined data for the Virgo, Fornax, and the Coma cluster, plus the two field samples from the RSA and from Sadler, are shown in Figure 4. The slope of the relation for galaxies brighter than $M_{B(T)} = -20$ is $dM/d \log R_e \sim -3$, showing that the $\langle SB \rangle_e$ for these galaxies becomes fainter for increasing luminosity; the radius is increasing faster with brightness than the constant surface brightness condition. The opposite is true for galaxies fainter than $M_{B(T)} \sim -19$. The equivalent diagrams to Figure 4 that show the $\langle SB \rangle$ correlation (rather than the radius correlation) with $M_{B(T)}$ are shown later as Figures 9–12. Figures 3 and 4 here are similar to Figure 7 of BST for their Virgo cluster data which they combined with other data from selected field galaxies.

Figure 4 shows that Hubble's (1926) scaling law of $m \sim -5 \log r''$ is valid only over the quite restricted magnitude range

TABLE 1

PHOTOMETRIC DATA FOR GALAXIES IN THE VIRGO CLUSTER

Eta	r"	B	<SB>
N4267 Vigroux et al.			
MBT=-19.90	re=	40.7	
Be=12.55	<SB>e	=21.8	
1.0	4.8	13.82	18.4
1.3	9.6	13.27	19.4
1.5	24.0	12.77	20.9
1.7	74.1	12.11	22.7
N4365 King			
MBT=-21.10	re=	66.1	
Be=11.35	<SB>e	=21.6	
1.0	28.8	12.05	20.5
1.3	81.3	11.35	22.1
1.5	162.2	11.18	23.4
1.7	199.5	11.00	23.7
2.0	323.6	10.86	24.6
2.5	537.0	10.79	25.6
N4365 Vigroux et al.			
MBT=-21.44	re=	104.7	
Be=11.01	<SB>e	=22.3	
1.0	25.1	11.97	20.2
1.3	81.3	11.13	21.9
1.5	107.2	10.97	22.3
1.7	141.3	10.84	22.8
2.0	204.2	10.69	23.4
N4374 King			
MBT=-21.47	re=	52.5	
Be=10.98	<SB>e	=20.8	
1.0	20.0	11.83	19.5
1.3	60.3	11.05	21.1
1.5	134.9	10.70	22.5
1.7	208.9	10.50	23.3
2.0	323.6	10.37	24.1
2.5	524.8	10.32	25.1
N4374 Vigroux et al.			
MBT=-21.50	re=	66.1	
Be=10.95	<SB>e	=21.2	
1.0	15.9	11.85	19.0
1.3	46.8	11.05	20.6
1.5	72.4	10.80	21.3
1.7	100.0	10.64	21.8
2.0	128.8	10.57	22.3
N4387 Vigroux et al.			
MBT=-19.30	re=	25.1	
Be=13.15	<SB>e	=21.3	
1.0	13.8	13.54	20.4
1.3	20.9	13.24	21.0
1.5	25.1	13.11	21.3
1.7	28.8	13.05	21.5
2.0	36.3	12.96	22.0
2.5	52.5	12.87	22.7
3.0	74.1	12.79	23.3
N4406 King			
MBT=-21.70	re=	93.3	
Be=10.75	<SB>e	=21.8	
1.0	26.3	11.70	20.0
1.3	100.0	10.86	22.1
1.5	218.8	10.50	23.4
1.7	316.2	10.32	24.0
2.0	467.7	10.23	24.8
N4406 Vigroux et al.			
MBT=-21.90	re=	100.0	
Be=10.55	<SB>e	=21.7	
1.0	50.1	11.20	20.9
1.3	104.7	10.64	21.9
1.5	147.9	10.45	22.5

Eta	r"	B	<SB>
N4459 Schombert			
MBT=-20.62	re=	44.7	
Be=11.83	<SB>e	=21.3	
1.0	17.8	12.50	19.9
1.3	31.6	12.06	20.8
1.5	66.0	11.60	21.9
1.7	87.0	11.47	22.4
2.0	126.0	11.30	23.0
2.5	190.6	11.20	23.8
3.0	295.0	11.14	24.7
3.5	371.5	11.11	25.2
N4472 King			
MBT=-22.60	re=	117.5	
Be= 9.85	<SB>e	=21.4	
1.0	39.8	10.85	20.0
1.3	117.5	9.95	21.5
1.5	199.5	9.66	22.4
1.7	309.0	9.42	23.1
2.0	407.0	9.35	23.6
2.5	603.0	9.27	24.4
3.0	759.0	9.27	24.9
3.5	1071.0	9.24	25.6
N4473 Jedrzjewski			
MBT=-20.76	re=	33.5	
Be=11.69	<SB>e	=20.5	
1.0	12.0	12.50	19.1
1.3	29.5	11.85	20.4
1.5	61.7	11.40	21.5
1.7	97.7	11.20	22.3
N4473 Vigroux et al.			
MBT=-20.70	re=	35.5	
Be=11.75	<SB>e	=20.7	
1.0	10.2	12.63	18.9
1.3	26.3	11.96	20.3
1.5	43.7	11.63	21.0
1.7	77.6	11.34	22.0
2.0	102.0	11.23	22.5
2.5	132.0	11.16	23.0
3.0	155.0	11.12	23.3
N4478 Jedrzjewski			
MBT=-19.55	re=	14.5	
Be=12.90	<SB>e	=19.9	
1.0	13.2	13.00	19.8
1.3	18.6	12.74	20.3
1.5	21.4	12.66	20.5
1.7	26.9	12.55	20.9
2.0	37.2	12.42	21.5
2.5	66.1	12.28	22.6
N4486 Schombert			
MBT=-22.08	re=	123.0	
Be=10.37	<SB>e	=22.0	
1.0	30.2	11.12	19.7
1.3	66.1	10.57	20.9
1.5	102.3	10.29	21.5
1.7	158.5	10.11	22.3
2.0	331.1	9.83	23.6
2.5	691.8	9.61	25.0
3.0	851.0	9.57	25.4

Eta	r"	B	<SB>
N4526 Fraser			
MBT=-21.37	re=	66.8	
Be=11.08	<SB>e	=21.4	
1.0	19.0	11.90	19.5
1.3	49.0	11.27	20.9
1.5	77.6	10.99	21.6
1.7	107.2	10.78	22.1
2.0	166.0	10.60	22.9
2.5	309.0	10.45	24.1
N4550 Vigroux et al.			
MBT=-19.47	re=	22.9	
Be=12.98	<SB>e	=21.0	
1.0	20.9	13.00	20.8
1.3	30.9	12.80	21.4
1.5	42.7	12.67	22.0
1.7	51.3	12.50	22.2
2.0	61.7	12.50	22.6
2.5	83.2	12.45	23.2
3.0	95.5	12.40	23.5
N4551 Vigroux et al.			
MBT=-18.84	re=	17.4	
Be=13.61	<SB>e	=21.0	
1.0	15.1	13.65	20.7
1.3	23.4	13.34	21.4
1.5	28.8	13.23	21.7
1.7	33.1	13.16	22.0
2.0	41.7	13.07	22.4
2.5	55.0	12.99	22.9
3.0	67.6	12.95	23.3
N4552 King			
MBT=-20.99	re=	31.6	
Be=11.46	<SB>e	=20.2	
1.0	12.9	12.40	19.1
1.3	26.9	12.27	20.6
1.5	46.8	11.50	21.0
1.7	93.3	11.20	22.2
2.0	251.2	10.95	24.1
N4578 Vigroux et al.			
MBT=-19.35	re=	37.1	
Be=13.10	<SB>e	=22.1	
1.0	9.1	13.94	19.9
1.3	63.1	12.52	22.7
1.5	74.1	12.43	23.0
1.7	81.3	12.38	23.1
2.0	87.1	12.35	23.2
2.5	107.2	12.30	23.6
N4636 Vigroux et al.			
Bt not available			
1.0	83.2	11.02	21.8
1.3	151.4	10.55	22.6
1.5	186.2	10.44	23.0
VC490 Vigroux et al.			
Bt not available			
1.0	12.0	17.47	24.1
1.3	18.2	17.17	24.7
V490/2 Vigroux et al.			
Bt not available			
1.0	28.2	14.84	23.3
1.3	33.9	14.70	23.5
1.5	40.7	14.59	23.8
1.7	47.9	14.50	24.1

Eta	r"	B	<SB>
VC545 Vigroux et al.			
Bt not available			
1.0	12.3	16.72	23.4
1.3	18.2	16.44	23.9
VC636 Vigroux et al.			
Bt not available			
1.0	6.8	17.92	23.3
1.3	9.6	17.66	23.8
1.5	11.8	17.54	24.1
VC1185 Vigroux et al.			
MBT=-16.30	re=	14.5	
Be=16.15	<SB>e	=23.2	
1.0	24.0	16.65	24.7
VC1254 Vigroux et al.			
MBT=-16.00	re=	12.8	
Be=16.45	<SB>e	=23.2	
1.0	18.6	16.13	23.7
1.3	26.3	15.85	24.1
1.5	29.5	15.78	24.3
1.7	30.9	15.76	24.4
VC1661 Vigroux et al.			
MBT=-17.20	re=	19.7	
Be=15.25	<SB>e	=22.9	
1.0	25.7	14.98	23.2
1.3	31.6	14.80	23.5
1.5	38.0	14.78	23.9
1.7	42.7	14.74	24.1
2.0	45.7	14.69	24.2
2.5	52.5	14.65	24.4
V1 Ichikawa,etal.			
MBT=-15.43	re=	10.8	
Be=17.02	<SB>e	=23.4	
1.0	14.8	16.79	23.8
1.3	20.0	16.56	24.3
1.5	23.4	16.47	24.5
1.7	25.1	16.43	24.6
2.0	26.9	16.40	24.7
V2 Ichikawa,etal.			
MBT=-15.36	re=	16.5	
Be=17.09	<SB>e	=24.4	
1.0	27.5	16.57	25.0
1.3	32.4	16.44	25.2
1.5	33.9	16.42	25.3
V3 Ichikawa,etal.			
MBT=-15.20	re=	6.7	
Be=17.25	<SB>e	=22.6	
1.0	7.9	17.09	22.8
1.3	10.2	16.93	23.2
1.5	12.0	16.81	23.4
1.7	13.2	16.77	23.6
2.0	17.0	16.67	24.0
2.5	20.0	16.62	24.3
V5 Ichikawa,etal.			
MBT=-14.03	re=	10.5	
Be=18.42	<SB>e	=24.7	

TABLE 1—*Continued*

Eta	r"	B	<SB>
V6 Ichikawa,etal.			
MBT=-16.74 re= 10.2			
Be=15.71 <SB>e =22.0			
1.0	12.0	15.62	22.2
1.3	16.6	15.39	22.7
1.5	20.0	15.28	23.0
1.7	24.5	15.18	23.3
2.0	31.6	15.09	23.8
2.5	39.8	15.02	24.2
V7 Ichikawa,etal.			
MBT=-13.37 re= 6.6			
Be=19.08 <SB>e =24.4			
1.0	12.0	18.98	25.6
1.3	13.2	18.91	25.7
V9 Ichikawa,etal.			
MBT=-14.98 re= 9.9			
Be=17.47 <SB>e =23.6			
1.0	15.1	17.11	24.2
1.3	20.0	16.91	24.6
1.5	21.4	16.85	24.7
1.7	23.4	16.81	24.9
2.0	24.5	16.79	24.9
V10 Ichikawa,etal.			
MBT=-15.87 re= 13.4			
Be=16.58 <SB>e =23.4			
1.0	17.0	16.38	23.7
1.3	27.5	16.04	24.4
1.5	31.6	15.94	24.6
1.7	33.1	15.92	24.7
2.0	37.2	15.87	24.9
V11 Ichikawa,etal.			
MBT=-14.01 re= 7.3			
Be=18.44 <SB>e =24.0			
1.0	10.5	18.09	24.4
1.3	15.5	17.83	25.0
1.5	16.7	17.79	25.1
1.7	17.4	17.76	25.2
V12 Ichikawa,etal.			
MBT=-12.78 re= 5.9			
Be=19.67 <SB>e =24.7			
1.0	10.2	19.11	25.4
1.3	11.5	19.01	25.5
V13 Ichikawa,etal.			
MBT=-15.47 re= 12.6			
Be=16.98 <SB>e =23.7			
1.0	15.9	16.80	24.0
1.3	26.3	16.41	24.7
1.5	30.2	16.34	24.9
1.7	31.6	16.33	25.0
2.0	33.1	16.30	25.1
V14 Ichikawa,etal.			
MBT=-14.01 re= 7.0			
Be=18.44 <SB>e =23.9			
1.0	11.2	18.04	24.5
1.3	14.1	17.85	24.8
1.5	15.5	17.80	24.9
1.7	15.9	17.79	25.0
2.0	16.6	17.76	25.1
V15 Ichikawa,etal.			
MBT=-15.92 re= 16.0			
Be=16.53 <SB>e =23.7			
1.0	24.0	16.16	24.3
1.3	33.1	15.92	24.7
1.5	36.3	15.86	24.9
1.7	38.0	15.83	24.9
2.0	39.8	15.81	25.0
V16 Ichikawa,etal.			
MBT=-13.70 re= 7.1			
Be=18.75 <SB>e =24.2			
1.0	12.0	18.31	24.9
1.3	15.1	18.13	25.2
1.5	16.2	18.08	25.3
V17 Ichikawa,etal.			
MBT=-13.81 re= 8.3			
Be=18.64 <SB>e =24.4			
1.0	14.8	18.05	25.1
1.3	16.2	17.99	25.2
1.5	17.4	17.95	25.3
V18 Ichikawa,etal.			
MBT=-16.05 re= 8.0			
Be=16.40 <SB>e =22.1			
1.0	9.1	16.26	22.3
1.3	12.9	16.01	22.8
1.5	15.0	15.93	23.0
1.7	16.2	15.88	23.1
2.0	20.0	15.81	23.5
2.5	23.4	15.76	23.8
3.0	24.5	15.75	23.9
V19 Ichikawa,etal.			
MBT=-15.51 re= 5.7			
Be=16.94 <SB>e =21.9			
1.0	6.3	16.88	22.1
1.3	8.5	16.64	22.5
1.5	10.0	16.55	22.7
1.7	11.8	16.48	23.0
2.0	15.1	16.38	23.5
2.5	20.0	16.30	24.0
V21 Ichikawa,etal.			
MBT=-15.38 re= 8.3			
Be=17.07 <SB>e =22.9			
1.0	10.7	16.88	23.2
1.3	14.1	16.65	23.6
1.5	17.4	16.53	23.9
1.7	20.4	16.45	24.2
2.0	23.4	16.39	24.4
V22 Ichikawa,etal.			
MBT=-16.74 re= 17.6			
Be=15.71 <SB>e =23.1			
1.0	24.0	15.45	23.5
1.3	33.1	15.22	24.0
1.5	39.8	15.12	24.3
1.7	44.7	15.06	24.5
2.0	47.9	15.02	24.6
2.5	52.5	15.00	24.8
V23 Ichikawa,etal.			
MBT=-12.95 re= 4.5			
Be=19.50 <SB>e =24.0			
1.0	7.2	19.05	24.5
1.3	8.5	18.93	24.8
1.5	9.3	18.87	24.9
1.7	10.0	18.83	25.0
V24 Ichikawa,etal.			
MBT=-15.72 re= 11.3			
Be=16.73 <SB>e =23.2			
1.0	12.3	16.69	23.3
1.3	17.8	16.43	23.9
1.5	27.5	16.16	24.6
1.7	31.6	16.10	24.8
2.0	33.9	16.06	24.9
V25 Ichikawa,etal.			
MBT=-16.23 re= 14.8			
Be=16.22 <SB>e =23.3			
1.0	19.5	16.01	23.7
1.3	28.8	15.71	24.2
1.5	33.1	15.64	24.4
1.7	37.2	15.58	24.6
2.0	40.7	15.53	24.8
V26 Ichikawa,etal.			
MBT=-13.52 re= 7.7			
Be=18.93 <SB>e =24.6			
1.0	13.5	18.43	25.3
1.3	16.2	18.26	25.5
V27 Ichikawa,etal.			
MBT=-14.80 re= 13.8			
Be=17.65 <SB>e =24.5			
V28 Ichikawa,etal.			
MBT=-13.67 re= 8.7			
Be=18.78 <SB>e =24.7			
1.0	14.8	18.25	25.3
1.3	16.6	18.13	25.4
V29 Ichikawa,etal.			
MBT=-17.77 re= 18.0			
Be=14.68 <SB>e =22.2			
1.0	23.4	14.51	22.6
1.3	31.6	14.29	23.0
1.5	37.2	14.19	23.2
1.7	42.7	14.13	23.5
2.0	51.3	14.05	23.8
2.5	63.1	14.00	24.2
3.0	67.6	13.98	24.3
V31 Ichikawa,etal.			
MBT=-15.67 re= 10.6			
Be=16.78 <SB>e =23.1			
1.0	5.0	17.41	22.1
1.3	24.5	16.29	24.4
1.5	30.2	16.17	24.8
1.7	32.4	16.13	24.9
2.0	34.7	16.11	25.0
V32 Ichikawa,etal.			
MBT=-15.11 re= 8.5			
Be=17.34 <SB>e =23.2			
1.0	10.7	17.15	23.5
1.3	15.9	16.88	24.1
1.5	20.0	16.74	24.4
1.7	20.9	16.71	24.5
2.0	24.0	16.66	24.8
V33 Ichikawa,etal.			
MBT=-17.44 re= 21.0			
Be=15.01 <SB>e =22.8			
1.0	23.4	14.97	23.0
1.3	40.7	14.57	23.8
1.5	52.5	14.42	24.2
1.7	63.1	14.33	24.5
2.0	67.6	14.30	24.6
V34 Ichikawa,etal.			
MBT=-12.73 re= 6.7			
Be=19.72 <SB>e =25.1			
1.0	12.3	19.08	25.7
V35 Ichikawa,etal.			
MBT=-15.66 re= 14.0			
Be=16.79 <SB>e =23.7			
1.0	19.5	16.49	24.1
1.3	29.5	16.18	24.7
1.5	32.4	16.30	25.0
1.7	33.9	16.11	25.0
2.0	37.2	16.07	25.1
V36 Ichikawa,etal.			
MBT=-16.21 re= 11.6			
Be=16.24 <SB>e =22.8			
1.0	14.1	16.07	23.0
1.3	20.9	15.80	23.6
1.5	26.3	15.67	24.0
1.7	30.9	15.58	24.2
2.0	33.1	15.56	24.4
2.5	38.0	15.51	24.6
V37 Ichikawa,etal.			
MBT=-16.70 re= 11.7			
Be=15.75 <SB>e =22.3			
1.0	12.6	15.74	22.4
1.3	19.0	15.43	23.0
1.5	23.4	15.33	23.4
1.7	28.2	15.22	23.7
2.0	38.0	15.11	24.2
2.5	46.7	15.06	24.6
V38 Ichikawa,etal.			
MBT=-14.76 re= 12.5			
Be=17.69 <SB>e =24.4			
1.0	21.9	17.22	25.1
1.3	25.1	17.11	25.3
1.5	26.3	17.08	25.4
V39 Ichikawa,etal.			
MBT=-14.13 re= 7.1			
Be=18.32 <SB>e =23.8			
1.0	12.6	17.94	24.6
1.3	15.5	17.78	24.9
1.5	16.2	17.75	25.0
1.7	17.0	17.72	25.1
V40 Ichikawa,etal.			
MBT=-13.73 re= 9.7			
Be=18.72 <SB>e =24.9			
1.0	17.0	18.09	25.4
1.3	19.5	17.98	25.6
V41 Ichikawa,etal.			
MBT=-14.06 re= 8.3			
Be=18.39 <SB>e =24.2			
1.0	13.2	17.93	24.7
1.3	17.8	17.73	25.2
1.5	18.6	17.69	25.2
V43 Ichikawa,etal.			
MBT=-15.49 re= 9.9			
Be=16.96 <SB>e =23.1			
1.0	12.9	16.75	23.5
1.3	18.2	16.49	24.0
1.5	23.4	16.36	24.4
1.7	25.1	16.32	24.5
2.0	28.8	16.25	24.7

TABLE 1—*Continued*

Eta	r"	B	<SB>
V45 Ichikawa,etal.			
MBT=-16.28 re= 19.4			
Be=16.17 <SB>e =23.8			
1.0	28.8	15.84	24.3
1.3	51.3	15.38	25.1
1.5	56.2	15.33	25.3
1.7	66.1	15.28	25.6
V46 Ichikawa,etal.			
MBT=-14.17 re= 9.1			
Be=18.28 <SB>e =24.3			
1.0	16.2	17.75	25.0
1.3	19.0	17.61	25.2
1.5	20.0	17.59	25.3
V47 Ichikawa,etal.			
MBT=-15.23 re= 13.2			
Be=17.22 <SB>e =24.0			
1.0	24.0	16.68	24.8
1.3	26.9	16.60	24.9
1.5	30.2	16.52	25.1
1.7	30.9	16.51	25.2
2.0	31.6	16.50	25.2
V48 Ichikawa,etal.			
MBT=-13.76 re= 7.7			
Be=18.69 <SB>e =24.3			
1.0	15.1	18.13	25.2
1.3	17.0	18.04	25.4
1.5	17.8	18.01	25.5
V50 Ichikawa,etal.			
MBT=-14.85 re= 12.8			
Be=17.60 <SB>e =24.3			
1.0	24.0	16.99	25.1
1.3	25.7	16.94	25.2
1.5	26.3	16.92	25.2
1.7	26.9	16.90	25.2
V53 Ichikawa,etal.			
MBT=-13.75 re= 6.9			
Be=18.70 <SB>e =24.1			
1.0	12.6	18.20	24.9
1.3	15.1	18.07	25.2
1.5	15.9	18.03	25.2
1.7	16.2	18.00	25.2
V54 Ichikawa,etal.			
MBT=-15.89 re= 8.7			
Be=16.56 <SB>e =22.5			
1.0	11.8	16.36	22.9
1.3	15.5	16.15	23.3
1.5	17.8	16.07	23.5
1.7	20.4	16.00	23.7
2.0	25.1	15.92	24.1
2.5	28.2	15.88	24.3
V55 Ichikawa,etal.			
MBT=-15.23 re= 8.1			
Be=17.22 <SB>e =23.0			
1.0	9.8	17.10	23.2
1.3	12.9	16.87	23.6
1.5	19.0	16.65	24.2
1.7	21.4	16.59	24.4
2.0	24.0	16.55	24.6
V56 Ichikawa,etal.			
MBT=-14.72 re= 10.9			
Be=17.73 <SB>e =24.1			
1.0	19.5	17.24	24.9
1.3	22.9	17.10	25.1
1.5	23.4	17.08	25.1
1.7	25.1	17.04	25.2
V57 Ichikawa,etal.			
MBT=-14.91 re= 10.5			
Be=17.54 <SB>e =23.9			
1.0	19.0	17.06	24.7
1.3	22.9	16.89	24.9
1.5	24.0	16.89	25.0
1.7	25.1	16.86	25.1
2.0	25.7	16.86	25.1
V59 Ichikawa,etal.			
MBT=-16.85 re= 22.1			
Be=15.60 <SB>e =23.5			
1.0	26.9	15.47	23.8
1.3	46.8	15.05	24.6
1.5	52.5	14.98	24.8
1.7	56.2	14.94	24.9
2.0	58.9	14.93	25.0
V60 Ichikawa,etal.			
MBT=-15.84 re= 12.7			
Be=16.61 <SB>e =23.3			
1.0	12.6	16.64	23.3
1.3	23.4	16.19	24.2
1.5	38.0	15.91	25.0
1.7	40.7	15.88	25.1
V62 Ichikawa,etal.			
MBT=-14.94 re= 10.1			
Be=17.51 <SB>e =23.7			
1.0	15.5	17.17	24.3
1.3	21.4	16.92	24.8
1.5	23.4	16.85	24.9
1.7	25.1	16.83	25.0
2.0	25.7	16.82	25.1
V63 Ichikawa,etal.			
MBT=-16.53 re= 11.9			
Be=15.92 <SB>e =22.5			
1.0	12.6	15.89	22.6
1.3	18.6	15.61	23.2
1.5	26.3	15.42	23.7
1.7	33.9	15.28	24.1
2.0	40.7	15.18	24.4
V64 Ichikawa,etal.			
MBT=-14.12 re= 11.4			
Be=18.33 <SB>e =24.8			
1.0	19.5	17.76	25.4
1.3	21.9	17.66	25.6
V65 Ichikawa,etal.			
MBT=-14.57 re= 11.0			
Be=17.88 <SB>e =24.3			
1.0	19.0	17.38	25.0
1.3	22.9	17.24	25.2
1.5	24.0	17.20	25.3
V66 Ichikawa,etal.			
MBT=-15.32 re= 10.3			
Be=17.13 <SB>e =23.4			
1.0	10.7	17.14	23.5
1.3	21.4	16.60	24.4
1.5	25.7	16.52	24.8
1.7	27.5	16.47	24.9
2.0	29.5	16.45	25.0
V69 Ichikawa,etal.			
MBT=-16.48 re= 12.4			
Be=15.97 <SB>e =22.6			
1.0	11.8	16.05	22.6
1.3	18.2	15.72	23.2
1.5	26.3	15.51	23.8
1.7	38.0	15.34	24.4
2.0	42.7	15.30	24.6

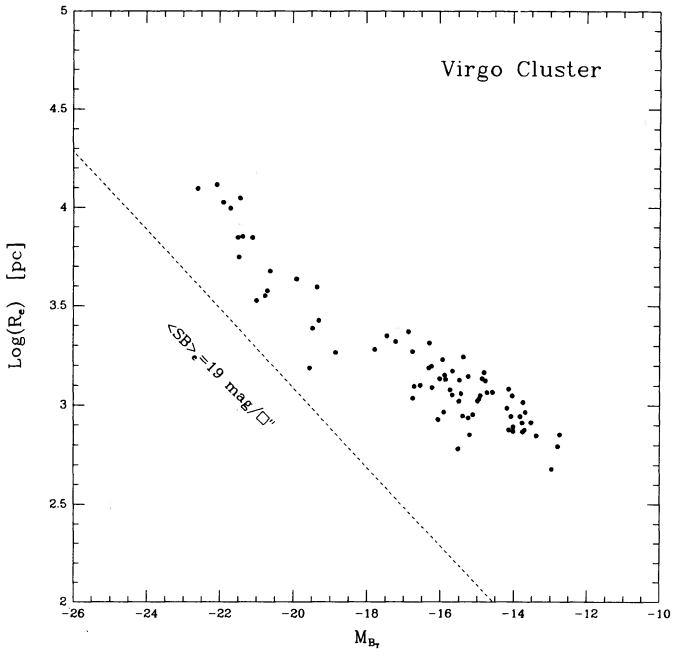

FIG. 3.—Variation of the linear effective radii R_e (in parsecs) with total blue absolute magnitude for Virgo cluster galaxies from the data in Table 1. The distance modulus of $m-M = 31.7$ is adopted for the cluster. A line of constant effective surface brightness ($\langle SB\rangle_e = 19$ mag arcsec^{-2}) is shown.

from -18.5 to -21.5 ($H_0 = 50$) (or M_T from -13.5 to -16.5 on Hubble's 1936 distance scale). By the circumstances of how Hubble chose his sample (mostly field galaxies from Hardcastle's 1914 list of 400 bright galaxies known at the time from inspection of the Franklin-Adams charts), this is simply the range of absolute magnitude which Hubble had access to. Galaxies neither from the very bright end of the luminosity function more luminous than $M_{B(T)} \sim -21.5$, *nor* the faint dwarfs were in his lists. Figure 4 shows that it is in these magnitude regimes that the deviation from the constant $\langle SB\rangle$ occurs, therefore unseen by Hubble.

Hubble's assumption that $m \sim -5 \log r''$ has dominated the literature for nearly half a century. The more recent discussions that the $dm/d \log r$ slope differs from -5 at the *faint* end began with Reaves (1956) and continued with Holmberg (1975), BST, Ichikawa, Wakamatsu, and Okamura (1986), Caldwell and Bothun (1987), Ferguson and Sandage (1988), Impey, Bothun, and Malin (1988), and undoubtedly by others.

From the first discussions by Oemler (1974, 1976) it became evident that $\langle SB\rangle$ decreases with increasing luminosity for the brightest galaxies. This was confirmed and extended by Kormendy (1977, 1980, 1982, 1987), Strom and Strom (1978*a*, *b*, *c*), Michard (1979), Thomsen and Frandsen (1983), BST, Cholonieswki (1985), Schombert (1986), Djorgovski and Davis (1987), and we suspect by others. Particularly striking illustrations of

TABLE 2

PHOTOMETRIC DATA FOR GALAXIES IN THE FORNAX CLUSTER

Eta	r"	B	<SB>
N1336 Schombert			
MBT=-18.95	re =		30.9
Be=13.70	<SB>e =		22.4
1.0	30.2	13.79	22.4
1.3	41.7	13.56	22.9
1.5	53.7	13.41	23.3
1.7	69.2	13.28	23.7
2.0	91.2	12.20	23.2
2.5	123.0	12.10	23.8
3.0	182.0	12.04	24.6
3.5	209.0	12.00	24.8
N1351 Schombert			
MBT=-19.40	re =		21.4
Be=13.25	<SB>e =		21.1
1.0	13.2	13.85	20.7
1.3	34.0	13.24	22.1
1.5	50.1	13.00	22.7
1.7	67.6	12.85	23.2
2.0	100.0	12.69	23.9
2.5	158.5	12.59	24.8
3.0	209.0	12.54	25.4
3.5	316.0	12.50	26.2
N1374 Schombert			
MBT=-19.95	re =		24.0
Be=12.70	<SB>e =		20.8
1.0	20.0	12.95	20.7
1.3	34.0	12.59	21.5
1.5	50.1	12.35	22.1
1.7	63.0	12.22	22.5
2.0	81.3	12.14	22.9
2.5	120.2	11.00	22.6
3.0	158.5	11.00	23.2
3.5	295.0	10.94	24.5
N1379 Schombert			
MBT=-19.90	re =		20.9
Be=12.75	<SB>e =		20.6
1.0	19.0	13.00	20.6
1.3	39.8	12.50	21.7
1.5	51.3	12.32	22.1
1.7	60.3	12.25	22.4
2.0	74.0	12.17	22.8
2.5	93.3	12.12	23.2
3.0	115.0	12.08	23.6
3.5	135.0	12.07	24.0
N1389 Schombert			
MBT=-19.70	re =		18.2
Be=12.95	<SB>e =		20.5
1.0	7.6	13.78	19.4
1.3	12.9	13.36	20.2
1.5	19.0	13.11	20.8
1.7	25.7	12.92	21.2
2.0	39.8	12.82	22.1
2.5	66.1	12.70	23.0
N1399 Hodge			
MBT=-21.60	re =		60.3
Be=11.05	<SB>e =		21.2
1.0	38.9	10.90	20.1
1.3	45.7	10.80	20.3
1.5	50.1	10.75	20.5
1.7	58.9	10.70	20.8
2.0	72.4	10.60	21.1
2.5	104.7	9.48	20.8
N1404 Hodge			
MBT=-21.34	re =		20.0
Be=11.31	<SB>e =		19.1
1.0	22.9	11.18	19.2
1.3	33.1	10.91	19.8
1.5	36.3	10.82	19.9
1.7	40.7	10.80	20.1
2.0	55.0	10.73	20.7
2.5	102.3	10.58	21.9
N1426 Schombert			
MBT=-19.80	re =		38.0
Be=12.85	<SB>e =		22.0
1.0	10.5	13.20	19.5
1.3	26.9	13.08	21.5
1.5	40.7	12.84	22.1
1.7	53.7	12.69	22.6
2.0	77.6	12.55	23.2
2.5	117.5	12.43	24.0
3.0	162.0	12.37	24.7
N1427 Schombert			
MBT=-20.10	re =		32.4
Be=12.55	<SB>e =		21.3
1.0	23.4	12.84	20.9
1.3	41.7	12.40	21.7
1.5	52.5	12.25	22.1
1.7	76.0	12.08	22.7
2.0	105.0	11.94	23.3
2.5	159.0	11.82	24.1
3.0	240.0	11.76	24.9
3.5	302.0	11.73	25.4
NG1 Caldwell			
MBT=-15.73	re =		13.2
Be=16.92	<SB>e =		23.8
1.0	13.5	16.87	23.8
1.3	24.0	16.56	24.7
1.5	26.3	16.50	24.8
1.7	30.2	16.48	25.1
2.0	43.7	16.37	25.8
NG4 Caldwell			
MBT=-15.65	re =		9.8
Be=17.00	<SB>e =		23.2
1.0	12.0	16.90	23.5
1.3	17.4	16.65	24.1
1.5	20.9	16.60	24.4
1.7	23.4	16.55	24.6
2.0	25.7	16.51	24.8
2.5	30.2	16.49	25.1
NG22 Caldwell			
MBT=-14.00	re =		12.6
Be=18.65	<SB>e =		25.4
1.0	18.2	18.28	25.8
1.3	21.9	18.21	26.2
1.5	14.0	18.15	25.1
1.7	26.3	18.07	26.4
2.0	30.2	18.05	26.7
2.5	34.7	18.00	26.9
NG24 Caldwell			
MBT=-16.95	re =		12.3
Be=15.70	<SB>e =		22.4
1.0	15.1	15.65	22.8
1.3	25.1	15.37	23.6
1.5	29.5	15.25	23.8
1.7	33.1	15.19	24.0
2.0	43.7	15.14	24.6
NG35 Caldwell			
MBT=-13.50	re =		7.8
Be=19.15	<SB>e =		24.8
1.0	10.5	18.80	25.1
1.3	13.5	18.70	25.6
1.5	15.9	18.65	25.9
1.7	18.2	18.60	26.1
2.0	20.0	19.55	27.3
2.5	25.1	18.50	26.7
3.0	30.2	18.47	27.1
NG47 Caldwell			
MBT=-16.15	re =		11.0
Be=16.50	<SB>e =		22.9
1.0	21.4	16.10	24.0
1.3	24.5	15.99	24.2
1.5	26.3	15.95	24.3
1.7	30.9	15.85	24.5
2.0	38.9	15.77	25.0
NG60 Caldwell			
MBT=-12.90	re =		6.6
Be=19.75	<SB>e =		25.1
1.0	10.0	19.31	25.6
1.3	12.3	19.25	25.9
1.5	12.6	19.24	26.0
1.7	13.2	19.22	26.1
NG63 Caldwell			
MBT=-14.10	re =		8.5
Be=18.55	<SB>e =		24.4
1.0	13.8	18.18	25.1
1.3	16.2	18.09	25.4
1.5	17.8	18.05	25.5
1.7	18.6	18.01	25.6
2.0	26.0	17.95	26.3
2.5	29.5	17.90	26.5
NG82 Caldwell			
MBT=-12.90	re =		7.9
Be=19.75	<SB>e =		25.5
1.0	12.6	19.35	26.1
1.3	15.9	19.25	26.5
1.5	17.0	19.17	26.6
1.7	17.4	19.16	26.6
2.0	18.2	19.15	26.7
2.5	20.4	19.14	26.9
G14 Caldwell			
MBT=-17.90	re =		16.6
Be=14.75	<SB>e =		22.1
1.0	25.1	14.40	22.6
1.3	30.9	14.38	23.1
1.5	33.1	14.35	23.2
1.7	38.0	14.24	23.4
2.0	41.7	14.20	23.5
2.5	50.1	14.15	23.9
G72 Caldwell			
MBT=-16.00	re =		13.5
Be=16.65	<SB>e =		23.5
1.0	17.4	16.40	23.8
1.3	25.1	16.12	24.4
1.5	30.9	16.09	24.8
1.7	33.9	16.05	24.9
2.0	39.8	15.96	25.2

the fainter SB for the brightest E galaxies are the photographs by Burbidge (1962) for NGC 6166 and its companions, and by Burbidge, Burbidge, and Crampin (1964) for the E pair of NGC 4782/83. These photographs gave one of the first indications of the larger effective radii for the brightest galaxies compared with the constant ⟨SB⟩ case.

b) Correlations Using Petrosian Parameters

We now inquire if the features in Figure 4 are also present in correlations that use the Petrosian metric radii listed in Tables 1–3, rather than effective radii. Figure 5 shows the data for the Virgo cluster alone for η values of 1.3, 1.7, 2.0, and 2.5 mag

TABLE 2A

ADDITIONAL PHOTOMETRIC DATA FOR GALAXIES IN THE FORNAX CLUSTER

Name (1)	Be (2)	MBT (3)	re" (4)	<SB>e (5)	Name (1)	Be (2)	MBT (3)	re" (4)	<SB>e (5)
N1419	14.35	-18.3	13.8	21.3	FCC90	15.75	-16.9	9.6	21.9
NG3	16.85	-15.8	15.1	24.0	FCC93	20.15	-12.5	8.7	26.1
NG5	17.55	-15.1	18.2	25.1	FCC94	20.05	-12.6	7.1	25.5
NG6	17.35	-15.3	12.6	24.1	FCC97	19.75	-12.9	9.4	25.9
NG7	16.25	-16.4	15.5	23.4	FCC99	17.85	-14.8	10.5	24.2
NG8	17.05	-15.6	14.5	24.1	FCC100	16.25	-16.4	16.8	23.6
NG9	17.65	-15.0	12.6	24.4	FCC103	20.05	-12.6	7.2	25.6
NG10	16.45	-16.2	20.4	24.2	FCC104	19.25	-13.4	8.3	25.1
NG11	16.95	-15.7	20.9	24.8	FCC105	18.05	-14.6	14.1	25.0
NG25	17.25	-15.4	14.1	24.2	FCC107	17.75	-14.9	9.3	23.8
NG29	18.15	-14.5	11.5	24.7	FCC108	19.85	-12.8	7.1	25.4
NG38	19.15	-13.5	7.9	24.9	FCC109	19.05	-13.6	8.8	25.0
NG44	17.35	-15.3	13.2	24.2	FCC110	17.55	-15.1	15.4	24.7
NG61	17.95	-14.7	10.7	24.3	FCC111	17.55	-15.1	13.0	24.4
NG69	15.75	-16.9	17.4	23.2	FCC114	20.45	-12.2	6.3	25.7
NG77	19.05	-13.6	6.9	24.5	FCC116	16.85	-15.8	13.4	23.7
NG80	16.95	-15.7	7.1	22.4	FCC117	18.95	-13.7	15.7	26.2
NG83	19.35	-13.3	10.0	25.6	FCC118	18.35	-14.3	9.1	24.4
NG102	20.45	-12.2	5.0	25.2	FCC100	16.25	-16.4	16.8	23.6
G8	14.75	-17.9	15.1	21.9	FCC125	19.45	-13.2	0.9	20.5
G26	16.21	-16.4	11.2	22.7	FCC126	21.15	-11.5	3.7	25.2
G43	16.65	-16.0	10.7	23.0	FCC127	20.55	-12.1	5.3	25.4
G75	15.95	-16.7	12.6	22.7	FCC131	21.05	-11.6	4.2	25.4
G79	15.95	-16.7	7.6	21.6	FCC132	19.25	-13.4	5.0	24.0
G84	15.15	-17.5	6.5	20.4	FCC133	18.25	-14.4	12.0	24.9
G91	15.25	-17.4	12.9	22.0	FCC134	18.35	-14.3	6.0	23.5
G92	16.65	-16.0	9.3	22.7	FCC136	15.55	-17.1	16.3	22.9
G103	13.95	-18.7	24.5	22.1	FCC137	17.65	-15.0	13.4	24.5
G104	16.45	-16.2	7.2	22.0	FCC138	19.35	-13.3	4.5	23.9
G118	15.65	-17.0	6.8	21.0	FCC140	19.75	-12.9	6.2	25.0
G142	16.25	-16.4	20.0	24.0	FCC141	20.45	-12.2	2.1	23.3
FCC25	18.45	-14.2	8.6	24.4	FCC142	19.25	-13.4	9.5	25.4
FCC27	20.05	-12.6	6.8	25.5	FCC143	15.05	-17.6	11.8	21.6
FCC30	19.65	-13.0	12.5	26.4	FCC144	19.95	-12.7	6.6	25.3
FCC31	17.55	-15.1	8.5	23.4	FCC145	20.35	-12.3	4.4	24.8
FCC32	16.15	-16.5	8.2	22.0	FCC146	20.25	-12.4	4.7	24.9
FCC34	19.15	-13.5	8.5	25.0	FCC149	20.65	-12.0	5.6	25.6
FCC36	16.65	-16.0	6.7	22.0	FCC150	16.45	-16.2	6.5	21.8
FCC38	18.25	-14.4	7.9	24.0	FCC151	18.75	-13.9	12.3	25.4
FCC40	18.35	-14.3	7.9	24.1	FCC154	19.95	-12.7	7.9	25.7
FCC42	19.05	-13.6	13.1	25.9	FCC155	19.05	-13.6	6.7	24.4
FCC46	16.35	-16.3	5.8	21.4	FCC156	17.95	-14.7	12.1	24.6
FCC48	17.85	-14.8	9.1	23.9	FCC157	19.05	-13.6	11.5	25.6
FCC49	19.95	-12.7	6.5	25.3	FCC158	17.55	-15.1	16.6	24.9
FCC50	17.35	-15.3	19.9	25.1	FCC159	18.85	-13.8	11.8	25.5
FCC51	19.25	-13.4	7.4	24.8	FCC160	18.45	-14.2	10.6	24.8
FCC52	19.25	-13.4	7.8	25.0	FCC163	20.55	-12.1	7.3	26.1
FCC54	18.75	-13.9	8.7	24.7	FCC165	18.25	-14.4	11.1	24.7
FCC56	18.25	-14.4	10.4	24.6	FCC166	18.85	-13.8	8.3	24.7
FCC57	18.55	-14.1	6.6	23.9	FCC168	19.45	-13.2	8.3	25.3
FCC58	18.75	-13.9	7.2	24.3	FCC171	18.65	-14.0	18.0	26.2
FCC59	20.15	-12.5	8.1	25.9	FCC172	21.15	-11.5	3.9	25.4
FCC61	18.75	-13.9	6.3	24.0	FCC174	17.45	-15.2	7.2	23.0
FCC63	13.45	-19.2	18.0	21.0	FCC175	19.55	-13.1	17.7	27.0
FCC65	18.25	-14.4	7.4	23.8	FCC178	17.95	-14.7	10.1	24.2
FCC66	17.65	-15.0	13.6	24.6	FCC181	17.95	-14.7	9.0	24.0
FCC68	17.25	-15.4	6.9	22.7	FCC185	20.25	-12.4	5.6	25.2
FCC70	19.25	-13.4	6.7	24.6	FCC187	18.25	-14.4	12.3	24.9
FCC71	21.25	-11.4	4.1	25.6	FCC188	16.85	-15.8	12.1	23.5
FCC73	20.15	-12.5	6.2	25.4	FCC189	19.55	-13.1	5.0	24.3
FCC74	18.45	-14.2	4.2	22.8	FCC191	20.05	-12.6	6.3	25.3
FCC75	20.55	-12.1	7.1	26.0	FCC192	20.35	-12.3	8.3	26.2
FCC77	18.95	-13.7	11.9	25.6	FCC194	18.95	-13.7	6.4	24.2
FCC79	19.45	-13.2	8.4	25.3	FCC195	17.45	-15.2	11.4	24.0
FCC80	16.35	-16.3	10.6	22.7	FCC196	18.45	-14.2	10.2	24.7
FCC81	17.85	-14.8	7.5	23.5	FCC197	19.85	-12.8	6.3	25.1
FCC82	17.15	-15.5	12.2	23.8	FCC198	18.65	-14.0	7.9	24.4
FCC84	20.25	-12.4	5.6	25.2	FCC200	18.15	-14.5	8.5	24.0
FCC85	17.05	-15.6	13.6	24.0	FCC201	17.45	-15.2	12.9	24.3
FCC86	18.25	-14.4	9.7	24.4	FCC202	16.05	-16.6	9.8	22.3
FCC87	19.35	-13.3	10.7	25.7	FCC203	16.25	-16.4	13.0	23.1
FCC89	18.75	-13.9	10.2	25.0	FCC206	16.55	-16.1	18.6	24.1

TABLE 2—*Continued*

Name (1)	Be (2)	MBT (3)	re" (4)	<SB>e (5)	Name (1)	Be (2)	MBT (3)	re" (4)	<SB>e (5)
FCC207	16.65	-16.0	8.5	22.5	FCC271	19.45	-13.2	7.5	25.1
FCC208	18.05	-14.6	11.7	24.6	FCC272	19.95	-12.7	9.9	26.2
FCC209	19.45	-13.2	6.7	24.8	FCC273	19.55	-13.1	7.1	25.0
FCC210	19.45	-13.2	7.9	25.2	FCC274	17.25	-15.4	12.0	23.9
FCC211	17.05	-15.6	5.6	22.0	FCC275	20.05	-12.6	7.7	25.7
FCC212	18.35	-14.3	15.2	25.5	FCC277	14.55	-18.1	10.1	20.8
FCC214	19.75	-12.9	6.2	25.0	FCC278	17.55	-15.1	6.0	22.7
FCC215	19.95	-12.7	7.4	25.5	FCC279	17.45	-15.2	14.0	24.4
FCC216	19.95	-12.7	6.9	25.4	FCC280	19.35	-13.3	8.3	25.2
FCC218	19.25	-13.4	7.6	24.9	FCC281	18.65	-14.0	10.4	25.0
FCC220	20.25	-12.4	5.6	25.2	FCC284	19.75	-12.9	10.4	26.1
FCC221	18.45	-14.2	6.0	23.6	FCC286	18.85	-13.8	6.3	24.1
FCC222	16.35	-16.3	14.5	23.4	FCC287	18.75	-13.9	9.2	24.8
FCC223	16.95	-15.7	16.6	24.3	FCC289	19.45	-13.2	7.3	25.0
FCC225	20.35	-12.3	5.7	25.4	FCC291	20.15	-12.5	7.5	25.8
FCC226	18.55	-14.1	18.5	26.1	FCC292	17.85	-14.8	10.0	24.1
FCC227	20.05	-12.6	7.3	25.6	FCC293	18.35	-14.3	10.4	24.7
FCC228	19.55	-13.1	9.2	25.6	FCC294	17.95	-14.7	13.1	24.8
FCC229	19.85	-12.8	6.8	25.3	FCC295	19.65	-13.0	7.1	25.1
FCC230	17.95	-14.7	8.2	23.8	FCC296	17.05	-15.6	10.8	23.5
FCC231	19.15	-13.5	8.3	25.0	FCC297	18.55	-14.1	13.3	25.4
FCC232	18.15	-14.5	9.0	24.2	FCC298	17.35	-15.3	7.6	23.0
FCC234	17.95	-14.7	13.3	24.8	FCC300	16.85	-15.8	16.4	24.2
FCC236	19.95	-12.7	5.7	25.0	FCC301	14.95	-17.7	12.4	21.7
FCC237	18.55	-14.1	8.9	24.5	FCC303	16.25	-16.4	13.5	23.1
FCC238	19.45	-13.2	8.9	25.4	FCC304	19.55	-13.1	9.7	25.7
FCC239	19.65	-13.0	5.4	24.5	FCC307	18.45	-14.2	15.3	25.6
FCC241	17.35	-15.3	15.9	24.6	FCC309	18.25	-14.4	19.1	25.9
FCC242	18.55	-14.1	11.0	25.0	FCC314	17.25	-15.4	14.7	24.3
FCC243	17.25	-15.4	11.7	23.8	FCC316	17.05	-15.6	15.4	24.2
FCC245	16.75	-15.9	12.9	23.5	FCC317	18.45	-14.2	8.9	24.4
FCC246	19.85	-12.8	8.5	25.7	FCC318	16.85	-15.8	15.8	24.1
FCC248	19.45	-13.2	4.9	24.1	FCC319	17.15	-15.5	14.8	24.2
FCC250	17.85	-14.8	9.4	24.0	FCC320	18.05	-14.6	6.6	23.4
FCC251	19.75	-12.9	8.6	25.7	FCC321	19.55	-13.1	12.2	26.2
FCC252	16.75	-15.9	11.1	23.2	FCC325	18.95	-13.7	7.8	24.6
FCC253	17.05	-15.6	10.8	23.5	FCC326	19.35	-13.3	7.4	24.9
FCC254	18.35	-14.3	11.8	25.0	FCC327	18.15	-14.5	11.7	24.7
FCC256	20.85	-11.8	4.5	25.4	FCC328	19.15	-13.5	10.9	25.6
FCC257	18.85	-13.8	6.7	24.2	FCC329	18.95	-13.7	5.5	23.9
FCC258	20.35	-12.3	6.8	25.8	FCC330	20.15	-12.5	4.6	24.7
FCC259	18.55	-14.1	13.6	25.5	FCC331	17.85	-14.8	19.2	25.5
FCC260	17.75	-14.9	14.9	24.9	FCC332	16.45	-16.2	8.3	22.3
FCC262	18.55	-14.1	9.2	24.6	FCC333	17.55	-15.1	6.0	22.7
FCC253	18.85	-13.8	13.2	25.7	FCC334	19.35	-13.3	6.8	24.8
FCC266	16.65	-16.0	5.6	21.6	FCC335	14.95	-17.7	12.9	21.8
FCC268	19.05	-13.6	7.1	24.5	FCC336	18.35	-14.3	7.8	24.0
FCC269	19.05	-13.6	12.2	25.7	FCC339	18.25	-14.4	10.4	24.6
FCC270	20.45	-12.2	5.4	25.4	FCC340	18.95	-13.7	5.7	24.0

arcsec^{-2}. The absolute magnitudes on the abscissae refer to the values using $m - M = 31.7$ for the distance modulus.

Similar data from Oemler's (1976) photometry for the Coma cluster are shown in Figure 6. The correlation of the *effective* radius versus total absolute blue magnitude is in the upper left panel. These data are to be compared with Figure 3 for Virgo. The Coma cluster is between 3.8 and 4.0 mag more distant than Virgo (Sandage and Tammann 1984; Dresseler 1984; Tammann and Sandage 1985; Tammann 1986); hence, only the brighter galaxies in the cluster are available from these data, in constrast to the deeper grasp into the Virgo cluster in Figure 3. The other three panels in Figure 6 show the correlation of Petrosian $r(\eta)$ radii with $M_{B(\eta)}$ for $\eta = 1.7$, 2.5, and 3.0 mag arcsec^{-2}, again for Coma galaxies. The steeper slope than -5 for $dM/d \log R$ is evident in all four panels of Figure 6.

A combination of the data for Virgo, Fornax, and Coma from Tables 1–5 is shown in Figure 7. Effective radii are used in the upper left panel. Petrosian $r(\eta)$ radii, listed at discrete values of η bteween 1.3 and 2.5 mag arcsec^{-2}, are used in the remaining five panels. The division into two branches with different slopes is again evident in each diagram.

As discussed in Paper I of this series, the purpose of using $r(\eta)$ radii rather than the effective radius has been to eliminate the necessity to extrapolate the $m(r)$ growth curve to $r = \infty$ that is needed to define B_T, and thereby to obtain r_e. A second reason is that the $r(\eta)$ radii are larger than r_e by the important factor of ~ 5 for $\eta = 3.0$ mag arcsec^{-2} (see SP90, Table 1 for the factors for other η values). Measurements of metric radii to large angular distances from the center are, of course, necessary if galaxies are to be observed to large enough redshifts to make the Tolman test practical by correcting for the seeing profile.

The data for the Virgo and Coma clusters are combined in Figure 8 which shows how well the various $r(\eta)$ radii are cor-

TABLE 3

PHOTOMETRIC DATA FOR GALAXIES IN THE COMA CLUSTER

Eta	r"	B	<SB>
N4816			
MBT=-22.50	re=	79.4	
Be=13.75	<SB>e	=24.5	
1.0	3.0	16.00	19.6
1.3	37.2	14.20	23.3
1.5	50.1	14.07	23.8
1.7	74.1	13.95	24.5
2.0	120.2	13.75	25.4
N4839			
MBT=-22.50	re=	75.9	
Be=13.75	<SB>e	=24.4	
1.0	10.0	15.14	21.4
1.3	37.2	14.12	23.2
1.5	52.5	13.92	23.8
1.7	91.2	13.66	24.7
2.0	166.0	13.45	25.8
N4840			
MBT=-20.74	re=	7.9	
Be=15.51	<SB>e	=21.3	
1.0	4.4	15.93	20.4
1.3	6.6	15.61	21.0
1.5	8.7	15.46	21.4
1.7	10.5	15.37	21.7
2.0	15.8	15.20	22.4
2.5	30.2	15.03	23.7
3.0	46.8	14.95	24.5
N4841			
MBT=-21.90	re=	23.4	
Be=14.35	<SB>e	=22.4	
1.0	7.9	15.13	20.9
1.3	24.5	14.30	22.5
1.5	33.9	14.11	23.0
1.7	49.0	13.92	23.6
2.0	58.9	13.85	23.9
2.5	72.4	13.80	24.3
3.0	91.2	13.77	24.8
N4864			
MBT=-20.90	re=	8.1	
Be=15.35	<SB>e	=21.1	
1.0	4.7	15.75	20.3
1.3	6.6	15.46	20.8
1.5	8.1	15.35	21.1
1.7	10.0	15.24	21.5
2.0	18.2	15.02	22.6
2.5	32.4	14.85	23.6
3.0	41.7	14.81	24.2
3.5	44.7	14.80	24.3
N4872			
MBT=-21.46	re=	17.0	
Be=14.79	<SB>e	=22.2	
1.0	6.0	15.49	20.6
1.3	12.0	15.00	21.6
1.5	20.0	14.70	22.4
1.7	29.5	14.50	23.1
2.0	50.1	14.30	24.0
2.5	64.6	14.23	24.5
3.0	91.2	14.16	25.2
N4874			
MBT=-23.47	re=	35.5	
Be=12.78	<SB>e	=21.8	
1.0	102.3	12.80	24.1
1.3	239.9	12.35	25.5
N4876			
MBT=-20.17	re=	5.1	
Be=16.08	<SB>e	=20.9	
1.0	4.3	16.23	20.6
1.3	6.0	15.97	21.1
1.5	7.8	15.82	21.5
1.7	8.3	15.79	21.6
2.0	10.5	15.69	22.0
2.5	14.1	15.60	22.6
3.0	20.9	15.54	23.4
N4881			
MBT=-20.95	re=	13.8	
Be=15.30	<SB>e	=22.2	
1.0	4.4	16.10	20.5
1.3	8.5	15.59	21.5
1.5	18.2	15.13	22.7
1.7	21.4	15.06	23.0
2.0	32.4	14.90	23.7
2.5	52.5	14.77	24.6
3.0	63.1	14.74	25.0
N4889			
MBT=-23.10	re=	36.3	
Be=13.15	<SB>e	=22.2	
1.0	12.9	14.10	20.9
1.3	31.6	13.39	22.1
1.5	39.8	13.08	22.3
1.7	49.0	12.98	22.7
2.0	74.1	12.68	23.3
N4906			
MBT=-20.19	re=	5.5	
Be=16.06	<SB>e	=21.0	
1.0	4.0	16.31	20.6
1.3	6.5	15.96	21.3
1.5	9.3	15.75	21.8
1.7	12.6	15.61	22.4
2.0	15.8	15.51	22.8
2.5	21.9	15.42	23.4
3.0	26.9	15.39	23.8
3.5	31.6	15.37	24.1
N4921			
MBT=-20.80	re=	12.6	
Be=15.45	<SB>e	=22.2	
1.0	5.5	16.02	21.0
1.3	8.3	15.71	21.6
1.5	14.8	15.37	22.5
1.7	24.5	15.13	23.3
2.0	37.2	14.95	24.0
2.5	45.7	14.89	24.4
3.0	63.1	14.84	25.1
N4926			
MBT=-21.41	re=	12.9	
Be=14.84	<SB>e	=21.6	
1.0	4.2	15.61	20.0
1.3	7.9	15.13	20.9
1.5	13.2	14.84	21.7
1.7	26.3	14.49	22.8
2.0	38.0	14.34	23.5
2.5	61.7	14.22	24.4
3.0	79.4	14.18	24.9
N4927			
MBT=-20.98	re=	10.5	
Be=15.27	<SB>e	=21.6	
1.0	5.9	15.70	20.8
1.3	9.5	15.33	21.5
1.5	13.5	15.12	22.0
1.7	20.0	14.92	22.7
2.0	28.8	14.79	23.3
2.5	43.7	14.67	24.1
3.0	66.1	14.60	24.9
N4952			
MBT=-21.64	re=	16.6	
Be=14.61	<SB>e	=22.0	
1.0	5.9	15.29	20.4
1.3	10.0	14.90	21.1
1.5	15.8	14.63	21.9
1.7	23.4	14.43	22.5
2.0	37.2	14.24	23.3
2.5	63.1	14.11	24.4
3.0	100.0	14.03	25.3
N4957			
MBT=-21.40	re=	17.0	
Be=14.85	<SB>e	=22.2	
1.0	6.6	15.51	20.9
1.3	12.3	15.05	21.7
1.5	23.4	14.67	22.8
1.7	30.9	14.54	23.2
2.0	50.1	14.33	24.1
2.5	72.4	14.22	24.8
3.0	85.1	14.20	25.1
Coma18			
MBT=-19.50	re=	7.1	
Be=16.75	<SB>e	=22.2	
1.0	4.5	17.10	21.6
1.3	7.2	16.74	22.3
1.5	10.2	16.52	22.8
1.7	13.2	16.40	23.2
2.0	17.8	16.28	23.8
2.5	23.4	16.20	24.3
3.0	27.5	16.18	24.6
Coma19			
MBT=-18.36	re=	3.0	
Be=17.89	<SB>e	=21.5	
1.0	3.2	17.86	21.6
1.3	4.6	17.57	22.1
1.5	5.2	17.49	22.3
1.7	6.3	17.40	22.6
2.0	7.6	17.32	23.0
2.5	9.1	17.27	23.3
3.0	10.2	17.24	23.5
Coma21			
MBT=-19.50	re=	2.6	
Be=16.75	<SB>e	=20.0	
1.0	2.5	16.80	20.0
1.3	3.2	16.50	20.2
1.5	3.8	16.45	20.6
1.7	4.7	16.35	20.9
2.0	5.5	16.30	21.2
2.5	7.9	16.20	21.9
3.0	10.5	16.20	22.5
3.5	13.5	16.20	23.1
Coma22			
MBT=-17.50	re=	2.6	
Be=18.75	<SB>e	=22.0	
1.0	2.3	18.83	21.9
1.3	4.0	18.43	22.7
1.5	5.0	18.28	23.0
1.7	5.9	18.22	23.3
2.0	6.6	18.16	23.5
2.5	8.3	18.10	23.9
3.0	9.5	18.07	24.2
Coma23			
MBT=-18.50	re=	5.4	
Be=17.75	<SB>e	=22.6	
1.0	2.9	18.25	21.8
1.3	5.4	17.73	22.6
1.5	8.1	17.47	23.3
1.7	10.0	17.37	23.6
2.0	13.2	17.26	24.1
2.5	17.0	17.19	24.6
3.0	22.4	17.13	25.1
Coma25			
MBT=-18.33	re=	2.8	
Be=17.92	<SB>e	=21.4	
1.0	1.0	18.64	19.9
1.3	2.5	17.99	21.2
1.5	4.4	17.65	22.1
1.7	5.9	17.50	22.6
2.0	7.6	17.41	23.1
2.5	10.5	17.32	23.7
3.0	14.1	17.27	24.3
Coma29			
MBT=-18.93	re=	2.0	
Be=17.32	<SB>e	=20.1	
1.0	1.0	17.85	19.1
1.3	2.4	17.22	20.4
1.5	3.2	17.02	20.8
1.7	4.3	16.89	21.3
2.0	5.9	16.78	21.9
2.5	7.8	16.70	22.4
3.0	9.8	16.66	22.9
3.5	14.5	16.62	23.7
Coma33			
MBT=-20.05	re=	7.9	
Be=16.20	<SB>e	=21.9	
1.0	2.5	17.11	20.4
1.3	6.2	16.44	21.6
1.5	9.8	16.17	22.4
1.7	15.5	15.93	23.1
2.0	18.6	15.86	23.5
2.5	30.9	15.72	24.4
3.0	42.7	15.66	25.1
Coma37			
MBT=-18.11	re=	3.4	
Be=18.14	<SB>e	=22.0	
1.0	3.2	18.20	21.9
1.3	4.9	17.90	22.6
1.5	5.6	17.80	22.8
1.7	6.3	17.73	23.0
2.0	7.9	17.60	23.3
2.5	9.8	17.50	23.7
3.0	11.0	17.45	23.9

TABLE 3—*Continued*

Eta	r"	B	<SB>
Coma38			
MBT=-18.50	re=		3.7
Be=17.75	<SB>e =		21.8
1.0	3.4	17.82	21.7
1.3	6.2	17.37	22.6
1.5	7.4	17.25	22.8
1.7	8.3	17.20	23.0
2.0	9.8	17.13	23.3
2.5	11.2	17.09	23.6
3.0	17.0	17.03	24.4
Coma40			
MBT=-18.74	re=		2.5
Be=17.51	<SB>e =		20.8
1.0	1.1	18.13	19.6
1.3	2.6	17.48	20.8
1.5	3.5	17.33	21.3
1.7	4.3	17.22	21.6
2.0	6.3	17.06	22.3
2.5	10.5	16.90	23.2
3.0	15.1	16.85	24.0
3.5	21.9	16.82	24.8
Coma41			
MBT=-18.83	re=		3.0
Be=17.42	<SB>e =		21.1
1.0	1.1	18.19	19.6
1.3	2.8	17.50	20.9
1.5	3.9	17.28	21.5
1.7	5.0	17.15	21.9
2.0	7.2	17.00	22.5
2.5	11.5	16.88	23.4
3.0	19.1	16.78	24.4
Coma48			
MBT=-19.06	re=		4.6
Be=17.19	<SB>e =		21.7
1.0	4.1	17.38	21.7
1.3	5.6	17.14	22.1
1.5	7.6	16.95	22.6
1.7	9.8	16.83	23.0
2.0	12.9	16.71	23.5
2.5	19.5	16.61	24.3
3.0	29.5	16.53	25.1
RB6			
MBT=-20.25	re=		4.2
Be=16.00	<SB>e =		20.3
1.0	4.0	16.05	20.3
1.3	6.5	15.80	21.1
1.5	8.3	15.65	21.5
1.7	10.0	15.52	21.8
2.0	12.3	15.47	22.2
2.5	14.8	15.45	22.5
3.0	17.4	15.40	22.8
RB31			
MBT=-18.15	re=		3.1
Be=18.10	<SB>e =		21.8
1.0	2.7	17.98	21.4
1.3	4.1	17.91	22.2
1.5	5.2	17.75	22.6
1.7	6.3	17.65	22.9
2.0	7.9	17.57	23.3
2.5	9.3	17.52	23.6
3.0	11.5	17.48	24.0
3.5	12.9	17.47	24.3
RB129			
MBT=-19.04	re=		5.2
Be=17.21	<SB>e =		22.1
1.0	3.2	17.56	21.3
1.3	4.7	17.28	21.9
1.5	6.9	17.04	22.5
1.7	9.8	16.87	23.1
2.0	11.7	16.80	23.4
2.5	19.5	16.65	24.3
3.0	21.4	16.63	24.5
RB195			
MBT=-17.80	re=		2.6
Be=18.45	<SB>e =		21.8
1.0	1.3	18.90	20.7
1.3	3.0	18.35	21.9
1.5	4.3	18.07	22.5
1.7	4.9	17.97	22.7
2.0	5.9	17.95	23.0
2.5	6.9	17.90	23.3
3.0	8.7	17.90	23.8
RB224			
MBT=-19.07	re=		3.5
Be=17.18	<SB>e =		21.1
1.0	3.1	17.30	21.0
1.3	4.2	17.04	21.4
1.5	5.1	16.92	21.7
1.7	6.9	16.77	22.2
2.0	9.1	16.67	22.7
2.5	11.5	16.61	23.2
3.0	13.2	16.60	23.4
3.5	19.1	16.54	24.2
RB241			
MBT=-20.40	re=		8.9
Be=15.85	<SB>e =		21.8
1.0	4.5	16.32	20.8
1.3	6.8	16.02	21.4
1.5	12.0	15.69	22.3
1.7	17.0	15.52	22.9
2.0	24.0	15.38	23.5
2.5	30.9	15.31	24.0
3.0	47.9	15.23	24.9
RB268			
MBT=-20.28	re=		18.6
Be=15.97	<SB>e =		23.6
1.0	4.3	17.10	21.5
1.3	17.8	16.00	23.5
1.5	22.9	15.85	23.9
1.7	25.1	15.79	24.0
2.0	43.7	15.58	25.0
IC382			
MBT=-20.68	re=		8.5
Be=15.57	<SB>e =		21.5
1.0	3.8	16.16	20.3
1.3	7.6	15.64	21.3
1.5	10.5	15.45	21.8
1.7	16.6	15.22	22.6
2.0	26.3	15.05	23.4
2.5	42.7	14.92	24.3
3.0	53.7	14.88	24.8
IC842			
MBT=-20.05	re=		7.2
Be=16.20	<SB>e =		21.7
1.0	3.0	16.81	20.4
1.3	5.0	16.43	21.2
1.5	10.0	16.01	22.3
1.7	13.8	15.85	22.8
2.0	19.5	15.70	23.4
2.5	29.5	15.59	24.2
3.0	38.9	15.54	24.7
I3957			
MBT=-20.11	re=		7.9
Be=16.14	<SB>e =		21.9
1.0	2.1	17.05	19.9
1.3	3.4	16.65	20.5
1.5	4.8	16.45	21.1
1.7	6.5	16.22	21.5
2.0	12.6	16.10	22.8
I3959			
MBT=-20.68	re=		12.0
Be=15.57	<SB>e =		22.2
1.0	6.3	15.91	21.2
1.3	8.1	15.77	21.6
1.5	12.0	15.57	22.2
1.7	20.4	15.37	23.2
I4051			
MBT=-21.06	re=		13.2
Be=15.19	<SB>e =		22.0
1.0	6.9	15.69	21.1
1.3	13.8	15.17	22.1
1.5	19.5	14.96	22.7
1.7	26.3	14.81	23.2
2.0	37.2	14.69	23.8
2.5	52.5	14.59	24.4
3.0	63.1	14.55	24.8
I4133			
MBT=-20.24	re=		5.2
Be=16.01	<SB>e =		20.9
1.0	1.7	16.82	19.3
1.3	3.3	16.38	20.2
1.5	4.7	16.18	20.8
1.7	7.6	15.95	21.6
2.0	13.2	15.70	22.5
2.5	24.5	15.57	23.8
3.0	39.8	15.47	24.7

related with r_e and also how the zero point of the correlation is offset relative to r_e for each η value. The agreement of the correlation between the clusters is excellent. The scatter of the correlations about the mean line is $\Delta(\log R) \lesssim 0.1$ dex. The factors by which r_e must be multiplied to obtain $r(\eta)$ are approximately 2, 2.5, 3.6, and 5.3 for $\eta = 1.5$, 2.0, 2.5, and 3.0, similar to the factors calculated for the various formal templates in the first paper of this series (SP90, Table 1). The factors for the de Vaucouleurs $r^{1/4}$ fitting template alone was discussed previously by Thomsen and Frandsen (1983, their Table V).

The difference in the slope of the data from that of the line of equality in Figure 8 for $\eta > 2$ shows that a common template $I(r)$ profile does not, in fact, fit E galaxies of all absolute magnitudes at large distances from the center. Galaxies with larger intrinsic radii (and therefore brighter absolute magnitudes) have more extended outer regions [in their ratio of $r(\eta)$ to r_e] than do fainter E galaxies. It is the same effect as discussed by Oemler (1974, 1976), Kormendy (1977), Malumuth (1983), and by Schomert (1987, 1988). Their statement that *the more luminous galaxies have extended envelopes* is equivalent to stating that the Oemler α/β ratios and/or the King r_t/r_c ratios increase as the absolute magnitudes brighten, giving thereby the change of slope from 1 in the data points in the lower two panels of Figure 8.

V. VARIATION OF SURFACE BRIGHTNESS AVERAGED OVER VARIOUS METRIC RADII FOR GALAXIES OF DIFFERENT ABSOLUTE MAGNITUDES

The data in the previous sections are now combined to determine how average SB values, suitably defined, vary with absolute magnitude. We use here both the effective and the Petrosian $r(\eta)$ radii to define the various $\langle SB \rangle$ measures. Both types of radii give *metric* rather than *isophotal* sizes; the dis-

TABLE 4

PHOTOMETRIC DATA FOR GALAXIES IN THE SADLER FIELD

Name	m−M	MBT	Be	re	<SB>e	Name	m−M	MBT	Be	re	<SB>e
N312	35.97	−22.47	14.25	22.8	22.28	N7117	35.22	−21.32	14.65	16.5	21.98
N323	35.95	−22.45	14.25	18.1	21.78	N7118	35.05	−21.35	14.45	18.1	21.98
N641	35.47	−22.37	13.85	23.8	21.98	N7192	33.71	−21.21	13.25	20.8	21.08
N745	35.32	−21.52	14.55	18.1	22.08	N7216	34.12	−20.62	14.25	15.7	21.48
N1419	32.18	−18.68	14.25	17.3	21.68	N7676	34.08	−20.68	14.15	12.5	20.88
N1930	34.54	−21.54	13.75	27.4	22.18	N7796	34.08	−21.48	13.35	18.1	20.88
N2305	34.04	−21.34	13.45	22.8	21.48	IC1459	32.64	−21.64	11.75	32.9	20.58
N2663	32.93	−21.23	12.45	72.0	22.98	IC1864	34.73	−21.23	14.25	16.5	21.58
N2887	33.58	−20.78	13.55	22.8	21.58	IC3370	33.67	−21.67	12.75	36.1	21.78
N3087	33.40	−20.80	13.35	18.9	20.98	IC4421	34.20	−20.40	14.55	9.1	20.58
N3136B	32.39	−18.89	14.25	15.0	21.38	IC4451	34.40	−21.50	13.65	31.4	22.38
N3224	33.65	−20.65	13.75	18.1	21.28	IC4889	33.43	−21.23	12.95	18.9	20.58
N5090	34.01	−20.81	13.95	15.7	21.18	IC4943	33.75	−19.85	14.65	9.1	20.68
N6483	34.90	−21.60	14.05	15.7	21.28	IC5105	35.16	−22.26	13.65	18.9	21.28
N6730	34.53	−21.23	14.05	14.4	21.08	107-G0	34.02	−21.12	13.65	19.8	21.38
N6758	34.08	−21.48	13.35	21.7	21.28	182-G0	34.95	−21.05	14.65	8.7	20.58
N6849	35.38	−21.98	14.15	22.8	22.18	208-G2	31.05	−18.85	12.95	25.0	21.18
N6861	33.72	−21.52	12.95	14.4	19.98	235-G4	34.90	−21.30	14.35	15.7	21.58
N6868	33.73	−22.03	12.45	34.4	21.38	235-G8	33.26	−19.16	14.85	9.9	21.08
N6909	33.63	−21.03	13.35	27.4	21.78	286-G4	35.06	−20.96	14.85	9.9	21.08
N6958	33.69	−21.29	13.15	19.8	20.88	286-G5	33.60	−20.00	14.35	16.5	21.68
N7002	35.86	−22.56	14.05	32.9	22.88	318-G2	34.79	−21.09	14.45	16.5	21.78
N7029	33.72	−21.22	13.25	16.5	20.58	323-G3	34.51	−22.01	13.25	21.7	21.18
N7097	33.46	−20.76	13.45	16.5	20.78						

tinction is highly important for the Tolman test (Sandage 1972).

Figure 9 shows the $\langle SB\rangle_e$, $M_{B(T)}$ relation for the Virgo cluster data in Table 1. The dwarf branch, defined as comprising galaxies fainter than $M_B \sim -19$, is well formed and shows *decreasing* ⟨SB⟩ with *decreasing* luminosity, again, as in BST (1984) and in Caldwell and Bothun (1987). The giant branch is ill defined using Virgo data alone because there are so few bright ellipticals in Virgo.

The sample is increased in Figure 10 by showing each of the data sets in turn for the Virgo plus the Fornax data from Tables 1 and 2 and 2A, for the Coma data from Table 3, and for the RSA2 galaxies from Table 5 and the Sadler field galaxy data from Table 4. The combined date are shown in Figure 11.[2]

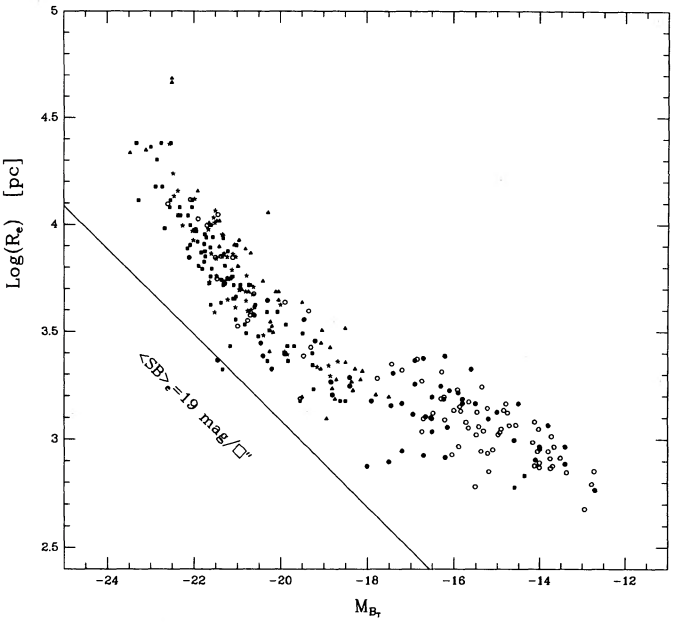

FIG. 4.—Same as Fig. 3, but with the data for the Fornax and Coma clusters added from Tables 2 and 3, combined with the data for the field galaxies from Tables 4 and 5. The Fornax data are calculated using the distance modulus of $m-M = 31.9$; those for Coma with $m-M = 35.5$, and those for the field data with the Hubble constant of 50 km s^{-1} Mpc^{-1}. Open circles are for the Virgo cluster, filled circles are for Fornax, filled triangles are for Coma, asterisks are galaxies studied by Sadler, and filled squares are the RSA2 field galaxy sample.

[2] Davies, Phillipps, and Disney (1989, and earlier references cited therein, hereafter DPD) state that the correlation in Fig. 11 does not exist. They believe that whatever correlation appears in diagrams similar to Fig. 11 is a selection effect. Because Fig. 11 is so central to applying the Tolman test, a comment is necessary here.

The data in Fig. 11 are for E and dE galaxy types alone. Adding spirals or background galaxies to the sample would degrade the correlation into a scatter diagram because, for different Hubble types, the ⟨SB⟩ becomes progressively fainter at a given absolute magnitude along the Hubble sequence (Sandage 1983). The effect on Fig. 11 of this variation of ⟨SB⟩ with Hubble type has been demonstrated by removing known background galaxies from a previous sample in the Fornax cluster used by Davies *et al.* (1988). Many galaxies considered by DPD as Fornax cluster members had been identified by Ferguson and Sandage (1988, hereafter FS88) as background spirals and brightest E glaxies in distant clusters. Their assessment was bsed on large-scale, high-resolution plates taken with the du Pont reflector at Las Campanas. Removing the contaminating spirals leaves only dE and dS0 galaxies, all considered by FS to be cluster members. These form a tight ⟨SB⟩, *M* diagram (FS88, Fig. 4) similar to Fig. 11. In addition, the galaxies which FS considered as background on the basis of morphology alone are uniformly spread over the area, whereas those which they assigned to the Fornax cluster on the same basis are concentrated toward the cluster center.

The galaxy sample which we are discussing in Fig. 11 is *complete* for E and dE galaxies in the Virgo and Fornax clusters within the ⟨SB⟩ range shown in the diagram. There are no low ⟨SB⟩ E and dE galaxies in the relevant absolute magnitude range. Galaxies with M_T between −24 and −17 with ⟨SB⟩ values between 23 and 26 mag $arcsec^{-2}$ would have been found in the catalog surveys of Virgo (Binggeli, Sandage, and Tammann 1985) and of Fornax (FS88, Ferguson 1989). What does not exist cannot lead to a noncorrelation in Fig. 11.

In their lists, Davies *et al.* (1988) and Davies, Phillipps, and Disney (1989) make no morphological distinction, nor do they have information on cluster membership or relative distances in their noncluster fields, clouding their claim that Fig. 11 for a complete sample would be a scatter diagram.

TABLE 5

PHOTOMETRIC DATA FOR GALAXIES IN THE RSA + RC2 SAMPLE

Name	m-M	MBT	Be	re	<SB>e	Name	m-M	MBT	Be	re	<SB>e
N 147	24.32	-14.36	10.71	190.8	23.8	N3818	32.05	-19.26	13.54	18.0	21.1
N 185	24.32	-14.59	10.48	169.2	23.2	N3872	33.88	-21.08	13.55	18.0	21.0
N 221	24.32	-15.53	9.54	32.4	18.7	N3904	32.13	-20.30	12.58	18.0	20.3
N 533	35.27	-22.52	13.50	43.2	22.6	N4168	31.70	-19.49	12.96	28.8	21.6
N 596	33.03	-21.15	12.63	28.8	21.2	N4261	33.09	-21.71	12.13	43.2	21.4
N 720	32.74	-21.59	11.90	36.0	21.0	N4278	30.37	-19.24	11.88	28.8	20.5
N 741	35.29	-22.75	13.29	43.2	22.4	N4283	31.62	-18.50	13.87	14.4	20.8
N 750	35.16	-21.99	13.92	18.0	22.2	N4365	31.70	-21.10	11.35	54.0	21.3
N 821	32.90	-21.01	12.64	43.2	21.9	N4374	31.70	-21.47	10.98	54.0	20.9
N1199	33.65	-21.23	13.17	21.6	21.2	N4373	34.00	-22.14	12.61	25.2	21.7
N1209	33.62	-21.36	13.01	21.6	20.4	N4473	31.70	-20.63	11.82	36.0	20.8
N1275	35.18	-23.27	12.66	25.2	21.5	N4476	31.70	-18.62	13.83	14.4	21.0
N1399	32.40	-21.61	11.54	28.8	20.1	N4478	31.70	-19.55	12.90	14.4	20.0
N1404	32.40	-21.34	11.81	14.4	19.1	N4486	31.70	-22.08	10.37	93.6	21.4
N1407	32.74	-21.81	11.68	36.0	20.7	N4494	32.01	-21.27	11.49	43.2	20.9
N1426	32.24	-19.87	13.12	25.2	21.2	N4564	31.70	-19.83	12.62	21.6	20.5
N1453	34.50	-21.91	13.34	21.6	21.2	N4621	31.70	-21.03	11.42	43.2	20.9
N1521	34.61	-22.03	13.33	32.4	22.0	N4660	31.70	-19.83	12.62	21.6	20.5
N1549	31.49	-20.79	11.45	32.4	20.4	N4696	33.66	-22.30	12.11	43.2	22.0
N1600	34.88	-22.87	12.76	32.4	21.7	N4782	34.39	-21.64	13.50	14.4	20.9
N1700	34.48	-22.67	12.56	25.2	21.0	N4783	34.74	-21.94	13.55	21.6	21.4
N2325	33.06	-21.28	12.53	32.4	21.7	N4889	35.56	-22.99	13.32	36.0	22.2
N2314	34.56	-21.73	13.58	18.0	21.2	N4936	33.93	-21.65	13.03	18.0	20.6
N2434	31.75	-19.68	12.82	25.2	21.4	N5044	33.48	-21.61	12.62	32.4	21.7
N2672	34.46	-21.95	13.26	25.2	21.5	N5077	33.55	-21.03	13.27	14.4	20.5
N2693	35.02	-22.32	13.45	25.2	21.7	N5322	32.95	-22.04	11.66	61.2	21.7
N2749	34.59	-21.56	13.78	21.6	21.7	N5557	34.09	-22.08	12.76	25.2	20.9
N2832	35.71	-23.32	13.14	36.0	22.3	N5576	32.27	-20.51	12.51	21.6	20.3
N2865	33.46	-21.37	12.84	18.0	20.5	N5638	32.51	-20.31	12.95	25.2	21.1
N2974	32.80	-21.12	12.43	32.4	21.3	N5813	32.78	-21.21	12.32	43.2	21.9
N2986	33.16	-21.32	12.59	25.2	20.8	N5831	32.53	-20.07	13.21	25.2	21.6
N3078	33.23	-21.31	12.67	25.2	21.0	N5982	33.92	-21.89	12.78	21.6	20.8
N3136	32.24	-20.82	12.17	25.2	21.0	N6721	34.68	-21.75	13.68	21.6	21.7
N3158	35.74	-22.84	13.65	28.8	22.0	N7014	34.88	-21.60	14.03	21.6	21.9
N3193	32.09	-20.26	12.58	25.2	21.0	N7144	33.07	-21.32	12.50	43.2	21.8
N3250	33.55	-21.76	12.54	32.4	21.7	N7145	32.86	-20.73	12.88	28.8	21.5
N3258	33.54	-21.06	13.23	18.0	21.2	N7507	32.53	-21.10	12.18	28.8	20.7
N3268	33.50	-20.93	13.32	21.6	21.5	N7619	34.53	-22.36	12.92	28.8	21.5
N3309	34.41	-21.76	13.40	18.0	21.3	N7626	34.30	-22.13	12.92	32.4	21.9
N3348	33.91	-21.83	12.83	25.2	21.2	N7785	34.54	-21.87	13.42	21.6	21.3
N3377	30.36	-19.26	11.85	43.2	21.2	I1459	32.57	-21.61	11.71	36.0	20.7
N3379	30.91	-20.58	11.08	57.6	20.9	I3370	33.65	-21.74	12.66	28.8	21.5
N3557	33.78	-22.55	11.98	43.2	21.5	I4296	34.15	-22.72	12.18	46.8	22.0
N3608	31.72	-19.84	12.63	25.2	21.0	I5105	35.14	-22.53	13.36	25.2	21.7
N3640	31.86	-20.60	12.01	36.0	21.1	HA85-2	33.60	-21.16	13.19	10.8	20.2

The Tolman test will be the search for the displacement faintward in the ordinate of Figure 11 by either 2.5 log $(1 + z)^4$ mag or 2.5 log $(1 + z)$ mag as the redshift increases, after the measured $\langle SB \rangle$ values of the distant galaxies have been corrected for the total K-term (i.e., the selective *plus the* $1 + z$ *band width nonselective term*; see Humason, Mayall, and Sandage 1956, Appendix A; Oke and Sandage 1968).

The turnover in the diagram near $M_{B(T)} \sim -20$ is a potentially valuable feature of Figure 11 because if distant cluster data can be obtained over the first five magnitudes (say) of the luminosity function, this turnover could be found observationally, and the abscissa values for each cluster need not be calculated from a cosmological model. Therefore, the test could be made independent of q_0, and of even the form of the Hubble diagram. But if the turnover cannot be found due to an insufficient flux grasp, the test would not be quite as clean in principle; $M_{B(T)}$ must be calculated for each (m, z) cluster data set, from (say) equation (33) of Sandage (1988), so as to find the abscissa $M_{B(T)}$ value in Figure 11. The result would then depend, but only very slightly, on the cosmology through q_0, despite the fact that the $(1 + z)^4$ factor is, itself, *model independent* (Sandage 1972). However, it needs to be pointed out that this dependence of the abscissa value in Figure 11 on q_0 is very small compared with the $(1 + z)^4$ factor, shown as follows.

Between the two limiting cosmological cases of $q_0 = 0$ and 1/2 (Ω between 0 and 1), the absolute magnitude *difference* calculated from the equation for the Hubble diagram in the standard cosmological model is 0.27 mag (see Sandage 1988, eqs. [41] and [42]). This uncertainty in the abscissa in Figure 11 for a distant cluster would be read as a displacement in the ordinate if the correlation line is moved horizontally in Figure 11. But as the slope of the correlation line is at most 1 (see Table 6 below), the uncertainty in $\langle SB \rangle$ caused by this lack of knowledge of $M_{B(T)}$ is at most ~ 0.3 mag. Note that there is no additional uncertainty in the $\langle SB \rangle$ ordinate because the calculation of $\langle SB \rangle$ will use only the directly observed apparent

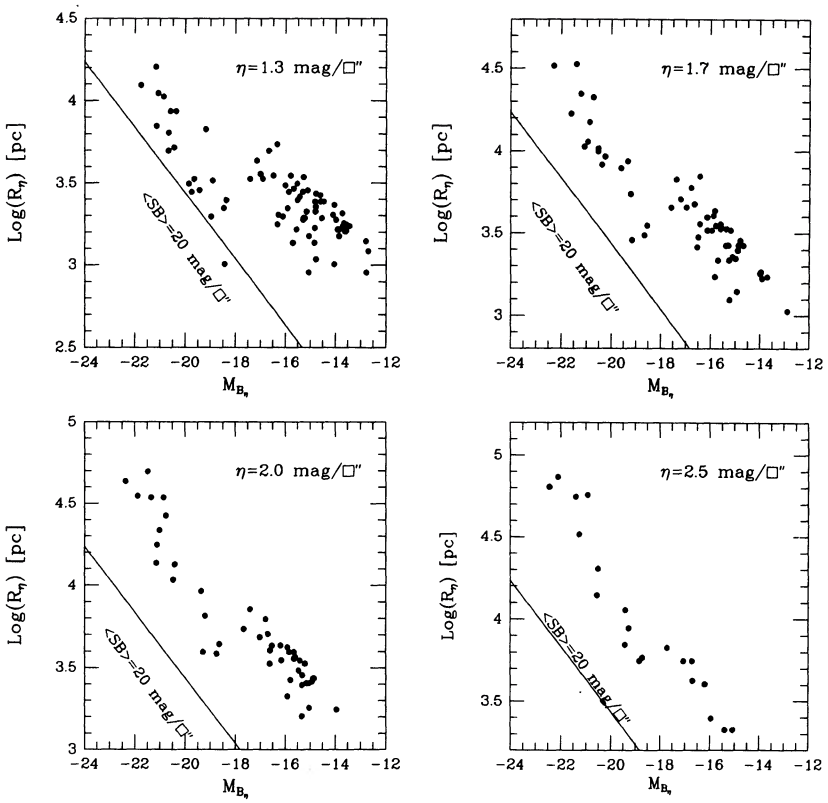

FIG. 5.—Correlation of the Petrosian $R(\eta)$ linear radii with the absolute magnitudes inside these respective radii for galaxies in the Virgo cluster from the data in Table 1, adopting $m-M = 31.7$ for the distance modulus. Data for four different values are shown.

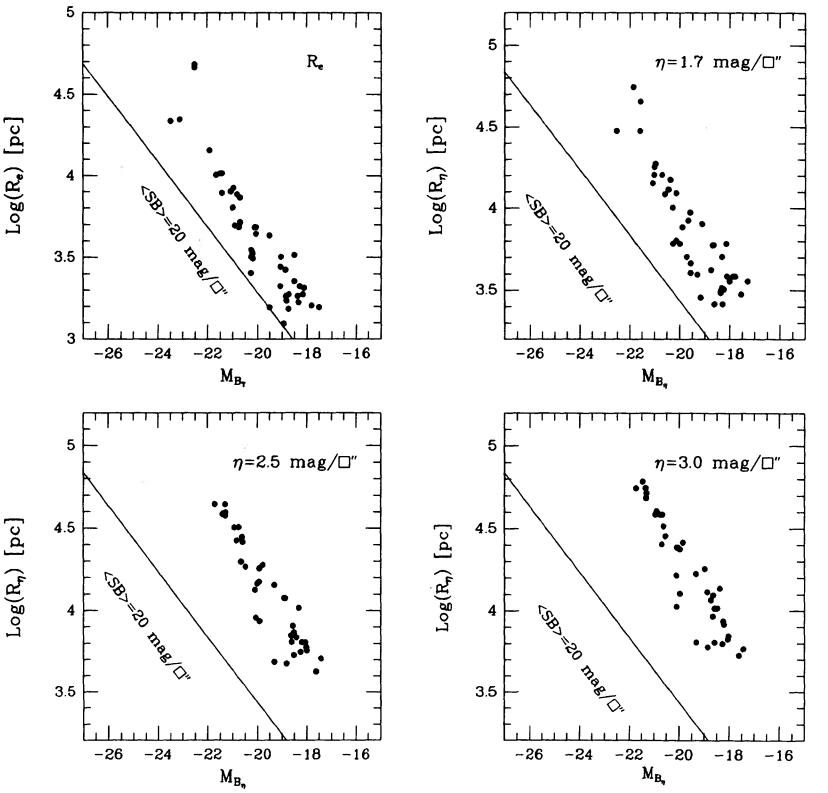

FIG. 6.—Same as Fig. 6, but for the Coma cluster for three values of η (using $M_{B(\eta)}$ for the abscissa), and for the effective radii (using total B magnitude for the abscissa), adopting $m-M = 35.5$ for the distance modulus. Lines of constant average surface brightness, using the appropriate M_B values are shown.

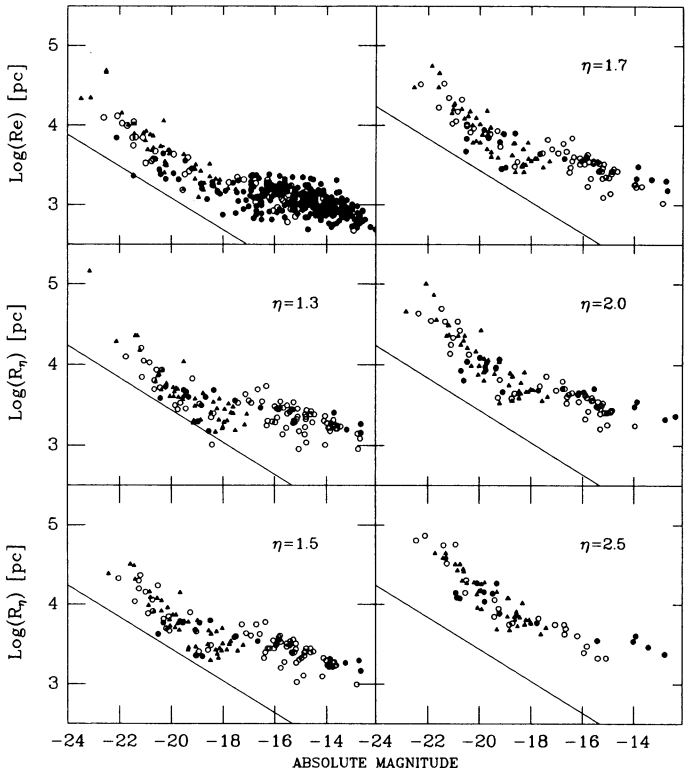

FIG. 7.—Similar to Figs. 5 and 6 but for the combined data for the Virgo, Fornax, and Coma clusters. Symbols have the same meaning as in Fig. 4. The straight line in each panel is the constant surface brightness condition.

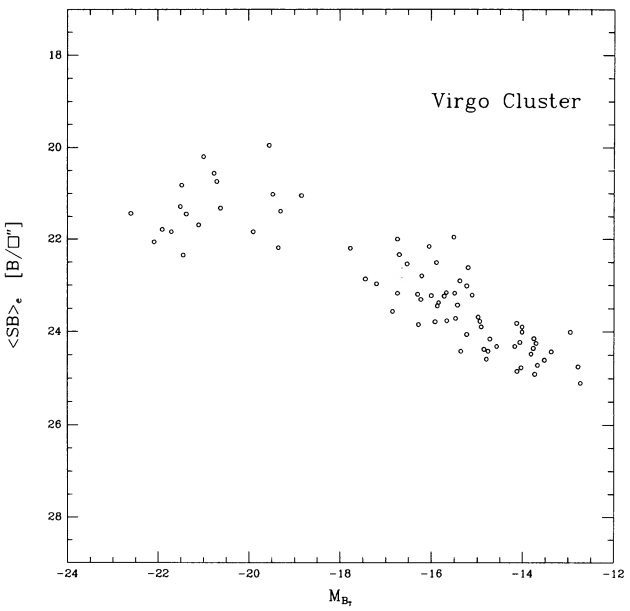

FIG. 9.—Correlation between the surface brightness averaged over the effective radius and the total blue absolute magnitude for Virgo cluster galaxies from Table 1.

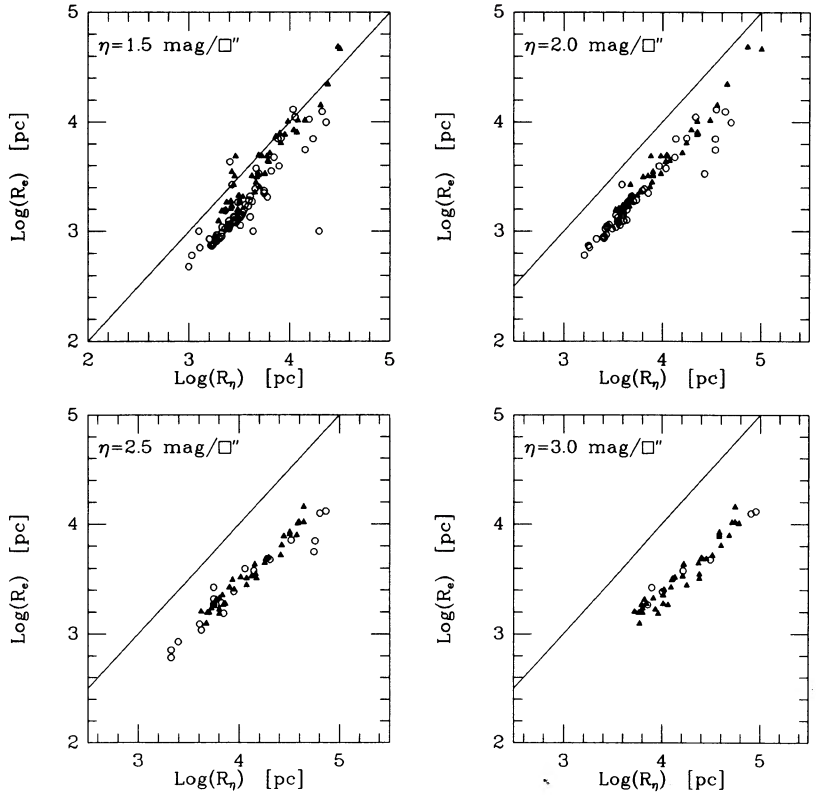

FIG. 8.—The relations between the effective linear radii and the Petrosian $R(\eta)$ radii for galaxies in the Virgo, Fornax, and Coma clusters for η values of 1.5, 2.0, 2.5, and 3.0 mag arcsec^{-2}. Same symbols as in Figs. 4 and 7. Data are from Tables 1 and 3. The drawn lines are for equality between ordinate and abscissa.

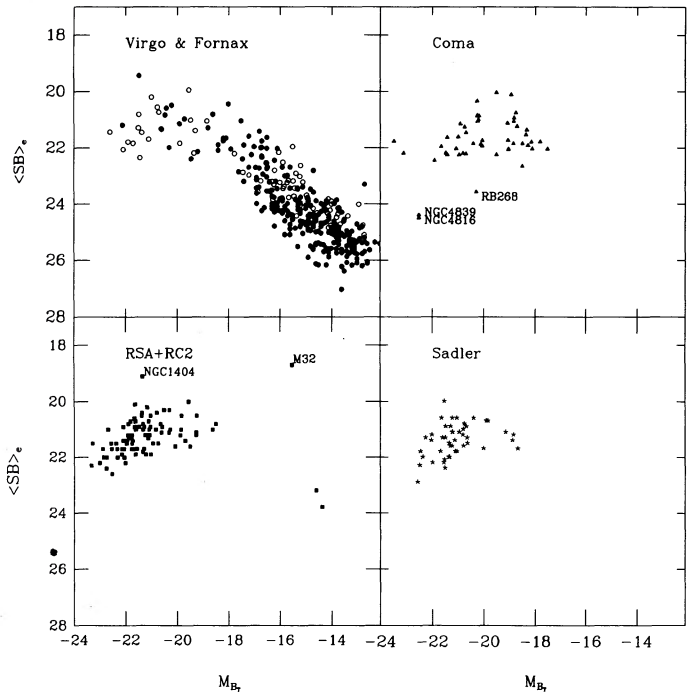

FIG. 10.—Same as Fig. 9, but for the separate data sets of Virgo plus Fornax, Coma alone, the RSA2 sample from Table 5, and the Sadler sample from Table 4.

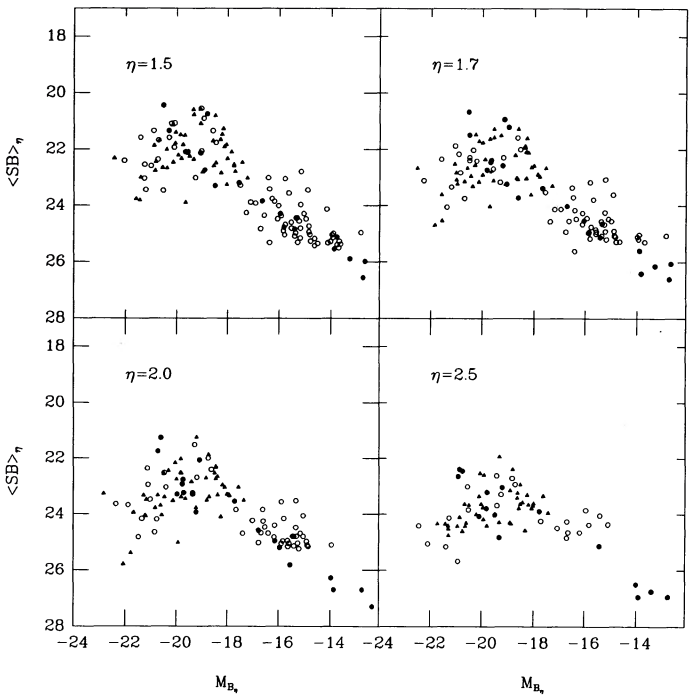

FIG. 12.—Same as Fig. 11, for Coma, Virgo, and Fornax, but using Petrosian parameters calculated for η values of 1.5, 1.7, 2.0, and 2.5 mag arcsec^{-2}.

magnitudes (K-corrected) and angular radii, both of which are measured, either at some Petrosian η radius or at the half-light radius. Hence, the uncertainty in M_T due to uncertainty in q_0 is small compared to the Tolman $(1 + z)^4$ factor of 1.8 mag at $z = 0.5$. Furthermore, as the redshift increases the Tolman factor increases relative to the model-dependent uncertainty in the abscissa due to an uncertain q_0 value. And even if the universe does not expand, and therefore if the standard model does not apply, our test would simply be to show that the Tolman factor for the *expanding* model could not be found.

Finally, we set out in Figure 12 the $\langle SB \rangle_\eta$, magnitude relation for four different Petrosian $r(\eta)$ radii using the combined data from Tables 1–3. The abscissa are $M_{B(\eta)}$ rather than "total" magnitude, circumventing the problem of extrapolating the growth curve to $r = \infty$. The second advantage of using Petrosian parameters is, again, the greater angular resolution they provide. However, the disadvantage is that the sampling at such large η values works in the regime of flux starvation at large redshifts.

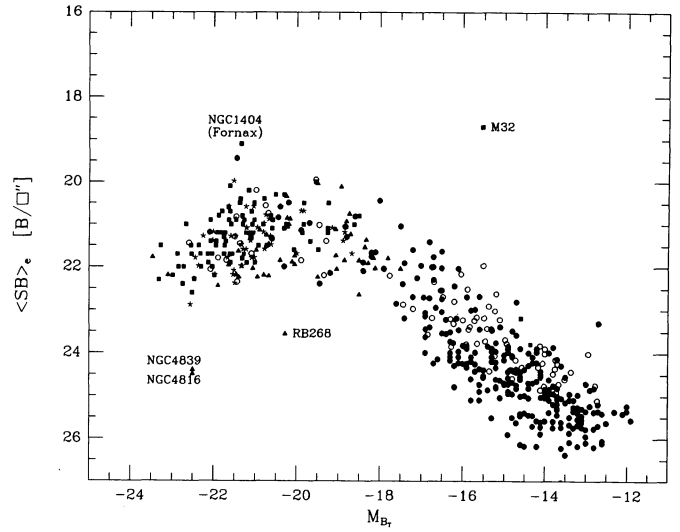

FIG. 11.—Correlation of effective surface brightness and absolute total B magnitude for the combined data from Tables 1–5. Symbols are the same as in Figure 4, 7, and 8. Note that these data are for E and dE galaxies only, with no contamination from later Hubble types which, if included, would produce a scatter diagram (N.B. footnote 2).

VI. INDEPENDENT CONFIRMATION OF THE ⟨SB⟩ DECREASE FOR INCREASING LUMINOSITY OF GIANT E GALAXIES

Because of the importance of Figure 11 and 12 for the Tolman test, we summarize here two modern independent studies which show that the sense of the bright-end slope of the ⟨SB⟩, M correlation in Figures 11 and 12 is correct.

The essence of the correlation had already been found in the prior works by Oemler (1974, 1976), by Kormendy (1977, 1980), and by Strom and Strom (1978*a*, *b*, *c*). They each have set out their data as a correlation between ⟨SB⟩ and R_e, not showing the absolute magnitude relation explicitly as in Figure 11, but, of course, implicitly because ⟨SB⟩ is derived from M and R alone. A review of much of this early work is given by Thomsen and Frandsen (1983) in the discussion of their photometry of the brightest E galaxies in two nearby galaxy groups and three clusters.

These authors fitted a de Vaucouleurs $r^{1/4}$ template to each

of their measured profiles. From the results listed in their Table II for the de Vaucouleurs r_e fitting parameter, it is possible to calculate $\langle SB \rangle_e$. (Thomsen and Frandsen list the SB *at* r_e. Their Table V, as well as Table 1 of SP90, shows that $\eta = 1.39$ mag arcsec^{-2} at r_e, which, when added to the SB at r_e gives $\langle SB \rangle_e$ averaged over the circular area of radius r_e.) We also calculate M_T from the redshift data, using $H_0 = 50$. Combining the $\langle SB \rangle$ and M data gives a diagram that is equivalent to Figure 11 here, but using only their data. The sense of fainter $\langle SB \rangle_e$ for brighter M_T is clearly seen in the reduced data of Thomsen and Frandsen. The slope, scatter, and zero-point closely resembles Figure 11. The data are of high weight, having been obtained and reduced digitally using a linear electronic image camera.

In a CCD study, Djorgovski and Davis (1987, their Table 1) give reduced data for a number of field E galaxies, also fitted with a de Vaucouleurs $r^{1/4}$ template, therefore giving, as in Thomsen and Frandsen, the fitting parameter r_e. Figure 13, shows their linear effective (not half-light) radius correlated with their listed absolute magnitude (reduced to $H_0 = 50$) in the R band. The line for the constant $\langle SB \rangle$ scaling law of $M \sim -5 \log R$ is shown. As in Figure 4 for our data, the brightest galaxies in the DD sample have fainter $\langle SB \rangle$ than those that are fainter; the radius increases more rapidly with luminosity than the constant SB case.

Figure 14 shows the data in Tables 1–5 in the $\langle SB \rangle$, log R_e plane in which Oemler, Kormendy, and Strom and Strom originally showed their data. The line, which is put with the slope found by DD from their data, clearly satisfies the Tables 1–5 data as well. The new feature of Figure 14., not seen in the original studies cited earlier, is the dwarf branch in this representation, showing again the *reverse* slope from the giant branch, breaking at $\langle SB \rangle_e \sim 20.5$ in B, and log R_e(psc) ~ 3.5, consistent with the two-branch relations in Figures 4, 7, and 10–12.

These tests with independent data obtained with linear electronic detectors are satisfactory in showing that the trends in the data plotted in Figures 11 and 12, which we analyze in the next section, are reliable.

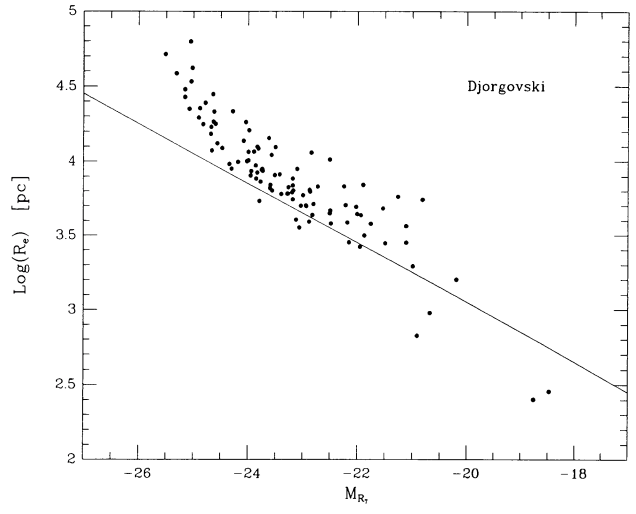

FIG. 13.—Independent data from Djorgovski and Davis (1987) for a sample of giant field E galaxies using their derived parameters (reduced to $H_0 = 50$). A line of constant surface brightness (slope $dM/d \log R = 5$) is shown. The four galaxies of high SB below the line are the compact (stripped?) galaxies M32, NGC 4486B, NGC 5845, and NGC 5846B.

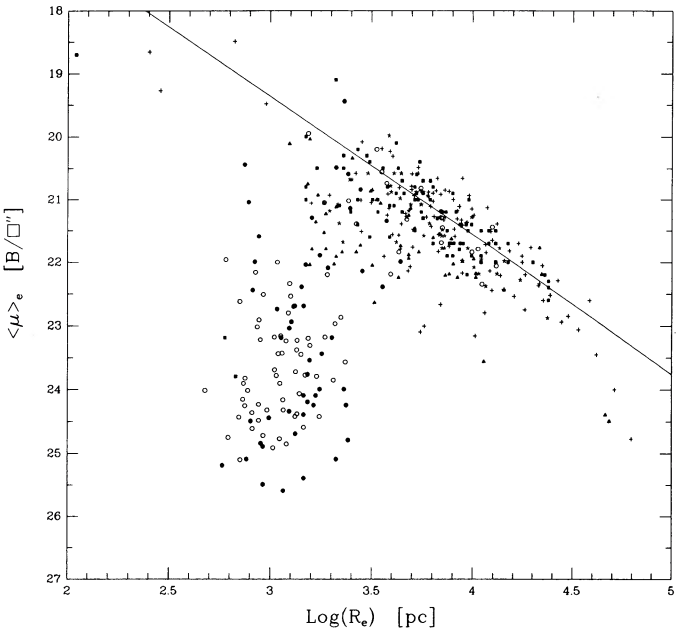

FIG. 14.—The $\langle SB \rangle$, log R_e diagram from the data used in the present paper from Tables 1–5. The line has the slope determined by Djorgovski and Davis from their independent data for giant galaxies.

VII. THE INTRINSIC SCATTER IN $\langle SB \rangle_e$ AND $\langle SB \rangle_\eta$ FOR GIANT E GALAXIES AT FIXED ABSOLUTE MAGNITUDE

We now inquire into the intrinsic dispersion of the correlation of $\langle SB \rangle$ and absolute magnitude. We envisage that the Tolman test will be made by measuring the $\langle SB \rangle$ of many galaxies in a given cluster of galaxies, sampling as deep as possible into the cluster's luminosity function. This is necessary because use of only the first-ranked member is inadequate since there is a spread of ~ 2 mag for known first-ranked galaxies (Sandage and Perelmuter 1991, in Paper III of this series), meaning that the first ranked in one cluster is not equivalent to the first ranked in any other to within this spread. We must therefore map segments of $\langle SB \rangle$, M diagram for each cluster, giving individual correlations similar to Figures 11 and 12 but displaced faintward by the Tolman effect by an amount dependending on the redshift.[3]

[3] In comparing the data of one cluster to those of others at different redshifts, we suppose that the abscissa (i.e., the absolute magnitude, corrected for K dimming due to redshift) can be determined. If the universe expands, eq. (33) of Sandage (1988) can be used. If it does not, we can simply use the observed tight relation between fully corrected apparent magnitude and redshift and assume a linear redshift-"photometric distance" relation at large redshifts, justified by its proof at small redshifts (Sandage and Hardy 1973, Fig. 7). If, on the other hand, the observations can be pushed faint enough to reach beyond the turnover in Fig. 11, the data can simply be compared by horizontal shifts of the apparent magnitude scale (again after K-correction) until the turnover parts of the separate diagrams are made to coincide. This approximation neglects the evolutinary effects discussed in Paper I, but which were estimated there to be small.

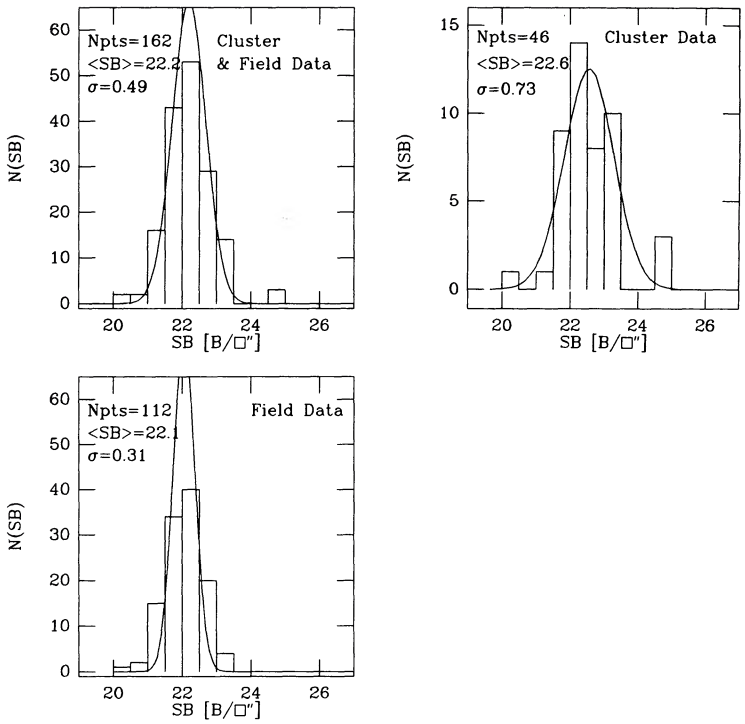

FIG. 15.—Distribution of the effective average surface brightness values for three data samples, after removing the correlation of ⟨SB⟩ with absolute magnitude that is tabulated in Table 6, and reducing the ⟨SB⟩ data to the absolute magnitude of $M = -22$ ($H_0 = 50$).

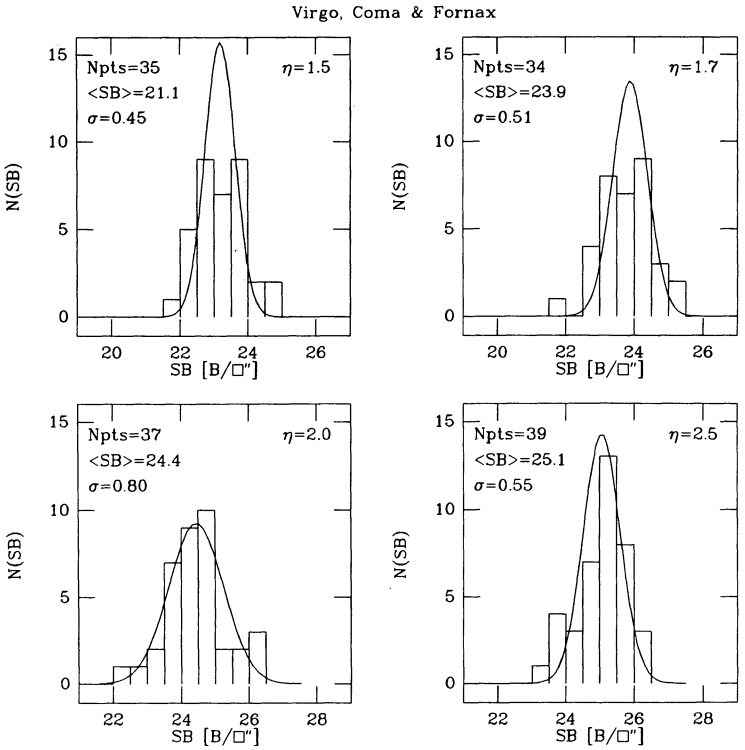

FIG. 16.—Same as Fig. 15, for Virgo, Coma, and Fornax, using Petrosian radii over which to average the surface brightnesses, again reduced to $M = -22$ for the absolute magnitude inside the particular $r(\eta)$ radius, by using the linear correlations set out in Table 6.

TABLE 6

LINEAR REGRESSIONS OF THE FORM $\langle SB \rangle = A(M_B) + C$ FOR THE CORRELATION OF SURFACE BRIGHTNESS AND ABSOLUTE MAGNITUDE OF GIANT GALAXIES FOR THE SAMPLES SHOWN IN FIGURES 11 AND 12

Radius Type (1)	Sample (2)	n (3)	A (slope) (4)	C (5)	Galaxies for $M_B < x$ (6)	sd (mag) (7)
Effective	cl + fld	162	−0.48	11.02	−20.00	0.49
Effective	cl only	46	−0.46	11.82	−20.00	0.73
Effective	fld only	116	−0.37	13.27	−20.00	0.31
Eta = 1.5	V + F + C	35	−0.43	13.34	−19.75	0.45
Eta = 1.7	V + F + C	34	−0.44	13.61	−19.75	0.51
Eta = 2.0	V + F + C	37	−0.46	13.90	−19.75	0.80
Eta = 2.5	V + F + C	39	−0.45	14.55	−19.25	0.55

Only the giant branches of each of the clusters are expected to be sampled in the test. The purpose of the present section is to determine the ratio of the intrinsic dispersion to the expected Tolman SB shift faintward along the ordinates in Figures 11 and 12 for these giant branches.

To this end, the mean correlation for the giant branches in Figures 11 and 12 have been calculated by least squares, with the results given in Table 6 for data using both Petrosian parameters and the effective $\langle SB \rangle$ and M_B values. These linear regressions permit the $\langle SB \rangle$ data to be *reduced to a fixed absolute magnitude*. The data in Tables 1–5 for galaxies brighter than the M values listed in column (6) of Table 6 have been reduced to $M = -22$ to take out the systematic variation of $\langle SB \rangle$ with absolute magnitude. The standard deviations have then been calculated for each case from the residuals about mean $\langle SB \rangle$ values, so reduced.

The results are shown in Figure 15 for the cluster and the field samples in Tables 1–5 using the effective radii as the measure of metric size. Similar results for the combined Virgo, Fornax, and Coma data are presented in Figure 16 using various Petrosian radii. Although there are significant differences in the calculated standard deviations (for reasons related to stochastic variations which are due to small sample size and to our inclusion in the calculation of a few highly deviant points), even the largest standard deviation of 0.80 mag is small compared to the expected Tolman effect at quite moderate redshifts. For example, at $z = 0.5$ the Tolman $(1 + z)^4$ factor is 1.8 mag. The effect is so large relative to the spread shown in Figures 15 and 16 that the Tolman effect should easily be found if it exists, even considering passive evolution in the look-back times.

If the large $(1 + z)^4$ shifts are not found when the high-redshift data become available, we shall then have a choice between denying the standard model or again invoking evolution (in this case it must be active rather than passive) as an adjustable parameter to save the theory. However, that decision is yet some distance ahead; in these first papers of the series our aim is simply to prepare the way by calibrating the local galaxies so as to form the base before venturing into the regime of large redshifts. The additional preparation that is required beyond that given here and in Paper I is the subject of Paper III on the calibration of the $\langle SB \rangle$ parameters for the *first few ranked galaxies* in many nearby clusters directly to provide an additional foundation upon which to compare the data expected in distant rich clusters.

REFERENCES

Binggeli, B., Sandage, A., and Tammann, G. A. 1985, *A.J.*, **90**, 1681.
Binggeli, B., Sandage, A., and Tarenghi, M. 1984, *A.J.*, **89**, 64 (BST).
Burbidge, E. M., 1962, *Ap. J.*, **136**, 1134.
Burbidge, E. M., Burbidge, G. R., and Crampin, D. J. 1964, *Ap. J.*, **140**, 1462.
Caldwell, N. 1987, *A.J.*, **94**, 1116.
Caldwell, N., and Bothun, G. 1987, *A.J.*, **94**, 1126.
Choloniewski, J. 1985, *M.N.R.A.S.*, **214**, 197.
Davies, J. I., Phillipps, S., and Disney, M. J. 1989, *M.N.R.A.S.*, **238**, 703.
Davies, J. I., Phillipps, S., Cawson, M. G. M., Disney, M. J., and Kibblewhite, E. J. 1988, *M.N.R.A.S.*, **232**, 239.
de Vaucouleurs, G., de Vaucouleurs, A., and Corwin, H. C. 1977, *Reference Catalogue of Bright Galaxies* (2d ed., Austin: University of Texas Press) (RC2).
Djorgovski, S., and Davis, M. 1987, *Ap. J.*, **313**, 59.
Dressler, A. 1984, *Ap. J.*, **281**, 512.
Ferguson, H. C. 1989, *A.J.*, **98**, 367.
Ferguson, H. C., and Sandage, A. 1988, *A.J.*, **96**, 1520.
Fraser, C. W. 1977, *Astr. Ap. Suppl.*, **29**, 161.
Hardcastle, J. A. 1914, *M.N.R.A.S.*, **74**, 699.
Holmberg, E. 1975, in *Galaxies and the Universe*, ed. A. Sandage, M. Sandage, and J. Kristian (Chicago: University of Chicago Press), pp. 123–157.
Hubble, E. 1926, *Ap. J.*, **64**, 321.
Humason, M. L., Mayall, N. U., and Sandage, A. 1956, *A.J.*, **61**, 97.
Ichikawa, S-I., Wakamatsu, K-I., and Okamura, S. 1986, *Ap. J. Suppl.*, **60**, 475.
Impey, C., Bothun, G., and Malin, D. 1988, *Ap. J.*, **330**, 634.
Jedrzejewski, R. 1987, *M.N.R.A.S.*, **226**, 747.
King, I. 1978, *Ap. J.*, **222**, 1.
Kormendy, J. 1977, *Ap. J.*, **218**, 333.
———. 1980, in *Proc. ESO Workshop on Two-dimensional Photometry*, ed. P. Crane and K. Kjar (Leiden: Sterrenwacht Leiden), p. 191.
———. 1982, in *Morphology and Dynamics of Galaxies, 12th Adv. Course of Swiss Soc. Astr. Ap.*, ed. L. Martinet and M. Major (Sauverny: Geneva Obs.), p. 115.
———. 1987, in *Nearly Normal Galaxies*, ed. S. M. Faber (New York: Springer), p. 163.
Longo, G., and de Vaucouleurs, A. 1983, *Univ. Texas Monogr. Astr.*, No. 3.
Longo, G., and de Vaucouleurs, A. 1985, *Univ. Texas Monogr. Astr.*, No. 3A.
Malumuth, E. M. 1983, Ph.D. thesis, University of Michigan.
Michard, R. 1979, *Astr. Ap.*, **74**, 206.
Oemler, A. 1974, *Ap. J.*, **194**, 1.
———. 1976, *Ap. J.*, **209**, 693.
Oke, J. B., and Sandage, A. 1968, *Ap. J.*, **154**, 21.
Reaves, G. 1956, *A.J.*, **61**, 69.
Sadler, E. 1984, *A.J.*, **89**, 34.
Sandage, A. 1972, *Ap. J.*, **173**, 485.
———. 1983, in *IAU Symposium 100, Internal Kinematics and Dynamics of Galaxies*, ed. E. Athanassoula (London: Reidel), p. 367.
———. 1988, *Ann. Rev. Astr. Ap.*, **26**, 561.
Sandage, A., and Hardy, E. 1973, *Ap. J.*, **183**, 743.
Sandage, A., and Perelmuter, J.-M., 1990, *Ap. J.*, **350**, 481.
———. 1991, *Ap. J.*, submitted.
Sandage, A., and Tammann, G. A. 1982*a*, *Ap. J.*, **256**, 339.
———. 1982*b*, in *Astrophysical Cosmology: Proceedings of the Vatican Study Week on Cosmology and Fundamental Physics*, ed. H. A. Bruck, G. V. Coyne, and M. Longair (Rome: Specola Vaticana), p. 23.
———. 1984, *Nature*, **307**, 326.
———. 1985, in *Lecture Notes in Physics*, Vol. **224**, *Supernova as Distance Indicators*, ed. N. Bartel (Berlin: Springer), p. 1.
———. 1987, *A Revised Shapley-Ames Catalog of Bright Galaxies, Carnegie Inst. Washington Pub.*, No. 635 (2d ed.; Washington, DC: Carnegie Institution of Washington) (RSA2).
Schombert, J. M. 1986, *Ap. J. Suppl.*, **60**, 603.
———. 1987, *Ap. J. Suppl.*, **64**, 543.
———. 1988, *Ap. J.*, **328**, 475.
Strom, S. E., and Strom, K. M. 1978*b*, *A.J.*, **83**, 732.
Strom, K. M., and Strom, S. E. 1978*a*, *A.J.*, **83**, 73.
———. 1978*c*, *A.J.*, **83**, 1293.
Tammann, G. A., and Sandage, A. 1985, *Ap. J.*, **294**, 81.
———. 1990, *Ap. J.*, in press.
Tammann, G. A. 1986, in *13th Texas Symposium on Relativistic Astrophysics*, ed. M. P. Ulmer (Singapore: World Scientific), p. 8.
Thomsen, B., and Frandsen, S. 1983, *A.J.*, **88**, 789.

Tolman, R. C. 1930, *Proc. Nat. Acad. Sci.*, **16**, 511.
———. 1934, in *Relatively Thermodynamics and Cosmology*, Oxford University Press (Oxford), § 180, 467.
Vigroux, L., Souviron, J., Lachieze-Rey, M., and Vader, J. P. 1988, *Astr. Ap. Suppl.*, **73**, 1.

JEAN-MARC PERELMUTER: Department of Physics and Astronomy. The Johns Hopkins University, Baltimore, MD 21218

ALLAN SANDAGE: The Observatories of the Carnegie Institution of Washington, 813 Santa Barbara Street, Pasadena, CA 91101